Journal of Medicinal Chemistry

Article

pubs.acs.org/jmc

# Selectivity, Cocrystal Structures, and Neuroprotective Properties of Leucettines, a Family of Protein Kinase Inhibitors Derived from the Marine Sponge Alkaloid Leucettamine B

Tania Tahtouh,[†] Jonathan M. Elkins,[‡] Panagis Filippakopoulos,[‡] Meera Soundararajan,[‡] Guillaume Burgy,[§,∥] Emilie Durieu,[†] Claude Cochet,[⊥] Ralf S. Schmid,[#] Donald C. Lo,[#] Florent Delhommel,[§] Anselm E. Oberholzer,[¶] Laurence H. Pearl,[◇] François Carreaux,[∥] Jean-Pierre Bazureau,[∥] Stefan Knapp,[‡] and Laurent Meijer*[,†,§]

[†]CNRS, "Protein Phosphorylation & Human Disease" Group, Station Biologique, 29680 Roscoff, Bretagne, France

[‡]University of Oxford, Nuffield Department of Clinical Medicine, Structural Genomics Consortium, Old Road Campus Research Building, Roosevelt Drive, Headington, Oxford OX3 7DQ, U.K.

[§]ManRos Therapeutics, Perharidy Research Center, 29680 Roscoff, Bretagne, France

[∥]Université de Rennes 1, Laboratoire Sciences Chimiques de Rennes, UMR CNRS 6226, Groupe Ingénierie Chimique & Molécules pour le Vivant (ICMV), Bât. 10A, Campus de Beaulieu, Avenue du Général Leclerc CS 74205, 35042 Rennes cedex, France

[⊥]INSERM U1036, "Biology of Cancer and Infection" Group, 38054-Grenoble, France

[#]Duke University Medical Center, Center for Drug Discovery and Department of Neurobiology, Durham, North Carolina, United States

[¶]Structural Biology Community Laenggasse (sbcl), CH-3000 Bern, Switzerland

[◇]University of Sussex, John Maynard Smith Building, Falmer, Brighton BN1 9QG, U.K.

Supporting Information

**ABSTRACT:** DYRKs (dual specificity, tyrosine phosphorylation regulated kinases) and CLKs (cdc2-like kinases) are implicated in the onset and development of Alzheimer's disease and Down syndrome. The marine sponge alkaloid leucettamine B was recently identified as an inhibitor of DYRKs/CLKs. Synthesis of analogues (leucettines) led to an optimized product, leucettine L41. Leucettines were cocrystallized with DYRK1A, DYRK2, CLK3, PIM1, and GSK-3$\beta$. The selectivity of L41 was studied by activity and interaction assays of recombinant kinases and affinity chromatography and competition affinity assays. These approaches revealed unexpected potential secondary targets such as CK2, SLK, and the lipid kinase PIKfyve/Vac14/Fig4. L41 displayed neuroprotective effects on glutamate-induced HT22 cell death. L41 also reduced amyloid precursor protein-induced cell death in cultured rat brain slices. The unusual multitarget selectivity of leucettines may account for their neuroprotective effects. This family of kinase inhibitors deserves further optimization as potential therapeutics against neurodegenerative diseases such as Alzheimer's disease.

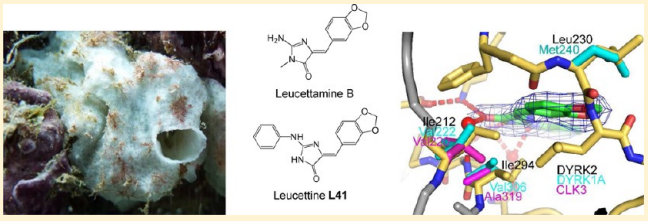


## INTRODUCTION

Protein phosphorylation on serine, threonine, and tyrosine residues by protein kinases represents probably the major post-translational mechanism used by cells to fine-tune their structural and regulatory proteins. Protein kinases represent a large class of enzymes comprising 518 members in man, probably over 2000 if alternative splicing is taken into account:[1] 90 tyrosine kinases, 388 serine/threonine kinases, and 40 sequences lacking a functional catalytic site. Phosphorylation abnormalities have been associated with numerous human diseases. Consequently, and following spectacular therapeutic and financial successes of the first marketed kinase inhibitors, protein kinases have become a major screening target, before G-protein coupled receptors, for the pharmaceutical industry in its search for novel therapeutic drugs.[2] However, only a small fraction of the 518 human kinases have been investigated as potential therapeutic targets.[3] Although cancer treatment is currently the main focus of these efforts, kinase inhibitors have a wide potential in most major diseases including neurodegenerative disorders, inflammation, cardiovascular and renal diseases, viral infections, etc. There are currently 258 inhibitors in the clinic (low molecular weight compounds and antibodies), mostly targeting tyrosine kinases and mostly targeting

Special Issue: Alzheimer's Disease

Received: July 15, 2012
Published: September 21, 2012





dx.doi.org/10.1021/jm301034u | J. Med. Chem. 2012, 55, 9312−9330

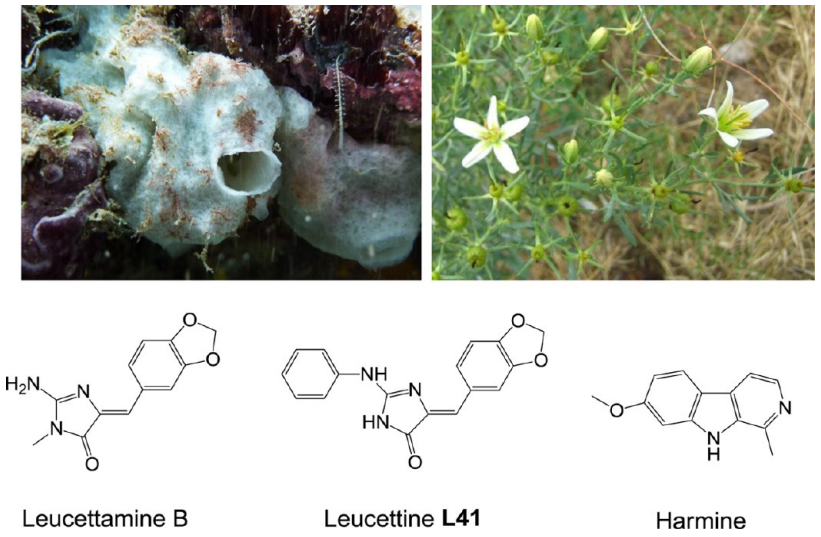


**Figure 1.** Structures of leucettamine B, leucettine L41, and harmine. Leucettamine is produced by the marine sponge *Leucetta microraphis* (*Calcarea*) (photography from Dr. Cécile Debitus, IRD), and harmine is extracted from the plant *Peganum harmala* (*Zygophyllaceae*) (Photography from Marck Menke in Stevens, P. F. (2001 onward). Angiosperm Phylogeny Web site, version 9, June 2008 http://www.mobot.org/MOBOT/research/APweb/ ).

cancer: 116 drugs are in clinical phase I, 82 in phase II, 37 in phase III, and 23 have reached the market.[2b]

While screening for low molecular weight inhibitors of DYRKs (dual specificity, tyrosine phosphorylation regulated kinases)[4] and CLKs (cdc2-like kinases),[5] we discovered that leucettines represented a promising family of inhibitors for these two closely related kinase classes.[6] Leucettines are derived from leucettamine B, a natural product initially isolated from the marine calcareous sponge *Leucetta microraphis* Hæckel (Figure 1).[7] Leucettamine B is chemically related to polyandrocarpamines,[8] dispacamide,[9] aplysinopsine,[10] clathridine,[7a,11] and hymenialdisine,[12] a series of alkaloids isolated from marine sponges. These molecules share a 2-aminoimidazolone core. Synthesis routes for leucettamine B[13] and analogues[6,14] have been reported. Similar to harmine, a reference DYRK1A inhibitor[15] initially isolated from the plant *Peganum harmala* (Figure 1),[16] leucettines inhibit both CLKs and DYRKs.[6]

We here investigated the selectivity of leucettine 41 using various approaches including two affinity chromatography methods. Results suggest that leucettine L41 interacts very specifically with DYRKs and CLKs but also with GSK-3, PIM1, CK2, and the lipid kinase PIKfyve. Most of these kinases are involved at different levels in the onset and development of Alzheimer's disease (AD). We also describe cocrystal structures of leucettine L41 with DYRK1A, DYRK2, CLK3, PIM1, and leucettine L4 with GSK-3$\beta$. We demonstrate that leucettine L41 inhibits DYRK1A and CLKs in a cellular context and displays neuroprotective properties. Leucettines thus constitute a promising scaffold for the design and optimization of selective pharmacological kinase inhibitors with potential applications to the treatment of AD.

## RESULTS

**Screening for Pharmacological Inhibitors of DYRKs and CLKs: Leucettamine B as an Inhibitory Scaffold.** To screen for pharmacological inhibitors of DYRKs and CLKs, DYRK1A and CLK1 were selected as the primary screening targets, while the other DYRKs and CLKs were used in secondary selectivity assays. Their kinase activities were assayed using the RS or woodtide peptide as a substrate and in the presence of 15 $\mu$M [$\gamma$-$^{33}$P]-labeled ATP. We first assayed a selection of 24 kinase inhibitors mostly derived from our laboratory (Supporting Information Table S1) and a small commercial library of 79 kinase inhibitors (Supporting Information Table S2). Results showed that a few well characterized kinase inhibitors also inhibited DYRK1A and CLK1 and suggested that selective DYRK1A and CLK1 inhibitors might be derived from some of these scaffolds which included indirubins, meriolins, and purines. In addition, most but not all DYRK1A inhibitors were efficient on CLK1 and many were active on PIM1. Harmine, a reference inhibitor for DYRK1A,[15a] also inhibited CLK1, while TG003, a reference CLK1 inhibitor,[17] inhibited DYRK1A (Supporting Information Table S1, Table 1). We also tested the five drugs which are or were used clinically for the treatment of AD (Donepezil, Galantamine, Memantine, Rivastigmine, and Tacrine) as well as a L'Oréal compound, which is structurally close to leucettines. None was found to be active on DYRKs and CLKs nor on any other kinase tested (Supporting Information Table S3).

A library of 40,000+ purified, low molecular weight compounds with high chemical diversity was screened in the DYRK1A/CLK1 medium throughput screen. This allowed the identification of a small number of inhibitory scaffolds including the expected harmine and some of its analogues.[16b] Among these scaffolds was leucettamine B, a natural product initially identified from marine calcareous sponges of the genus *Leucetta*.[7] We next set up a green chemistry method for the synthesis of leucettamine B and analogues, collectively referred to as leucettines.[6,14] From over 450 analogues synthesized and tested on DYRK1A and CLK1, we selected leucettine L41 as a representative, potent inhibitor of both kinases and used leucettamine B and harmine as reference compounds (Figure 1).

**Selectivity of Leucettine L41. (1) Protein Kinase Screens.** To investigate the selectivity of leucettine L41, we first screened the three compounds against a panel of 27 purified kinases, which included various forms of DYRK1A (recombinant enzymes from different species and native rat

**Table 1. Protein Kinase Selectivity of Leucettamine B, Leucettine L41, and Harmine[a]**

| kinases | leucettamine B | leucettine L41 | harmine |
|---|---|---|---|
| CDK1/cyclin B | >10 | >30 | 18 |
| CDK2/cyclin A | >10 | >30 | >30 |
| CDK5/p25 | >10 | >30 | 8 |
| CDK7/cyclin H | >10 | >10 | >10 |
| CDK9/cyclin T | >10 | 18 | 0.72 |
| CK1$\delta/\varepsilon$ | >10 | 30 | 1.8 |
| CK2 | −(10) | 0.32 | −(10) |
| CLK1 | 0.066 | 0.071 | 0.072 |
| CLK2 | 2.1 | 0.72 | 0.28 |
| CLK3 | 1.8 | >10 | >10 |
| CLK4 | 0.15 | 0.064 | 0.050 |
| DYRK1A (*R.n.*, ΔCt) | 0.92 | 0.040 | 0.056 |
| DYRK1A (native, *R.n.* brain) | 0.9 | 0.010 | 0.034 |
| DYRK1A (*H.s.*, FL) | 0.60 | 0.060 | 0.085 |
| DYRK1A (*H.s.*, ΔCt) | 0.95 | 0.055 | 0.060 |
| DYRK1B | 4.1 | 0.044 | 0.028 |
| DYRK2 | 2.0 | 0.073 | 0.120 |
| DYRK3 | 1.4 | 0.320 | 0.210 |
| DYRK4 | >10 | 0.52 | 9.5 |
| ERK2 | >10 | >30 | >30 |
| GSK-3$\alpha$ (*H.s.*) | 7.7 | 0.21 | >10 |
| GSK-3$\beta$ (*H.s.*) | >10 | 0.38 | >10 |
| GSK-3$\alpha/\beta$ (*S.c.*) | 2.9 | 0.41 | 19 |
| PIM1 | >10 | 1.5 | >10 |
| PfGSK-3 | −(10) | >10 | >10 |
| LmCK1 | −(10) | ≥10 | ≥10 |

[a]Leucettamine B, leucettine L41, and harmine were tested at various concentrations on 26 purified kinases as described in the Experimental Procedures. $IC_{50}$ values, calculated from the dose−response curves, are reported in μM. *H.s.*, *Homo sapiens*; *R.n.*, *Rattus norvegicus*; *S.c.*, *Sus scrofa*; PfGSK-3, *Plasmodium falciparum* GSK-3; LmCK1, *Leishmania major* CK1.

brain DYRK1A). $IC_{50}$ values were determined from dose−response curves (Table 1). The results showed consistently similar inhibition rates for all isoforms of DYRK1A by leucettine L41 and harmine, almost equal potency on DYRK1B and DYRK2, and slightly reduced inhibition values for the DYRK3 and DYRK4 isozymes. Leucettine L41, but not harmine, showed some inhibitory activity toward GSK-3, while harmine, but not leucettine L41, displayed some inhibition of CK1$\delta/\varepsilon$ (Table 1). Modest inhibition of CK2 was also observed for leucettine L41 but not for leucettamine B and harmine. Selectivity of leucettine L41 was also assessed by screening it against the Dundee University kinase panel (76 kinases) (Supporting Information Table S4), confirming the inhibition of DYRKs and adding weak cross-reactivity with the related kinases HIPK2, PIM3, and CK2. To complement the selectivity studies, the three compounds were screened on the large scale DiscoverX KinomeScan panel (Figure 2, Supporting Information Table S5). This interaction assay provides an overall view of the affinity of a compound for any of 402 kinases.[18] A semiquantitative scoring of this primary screen was provided in addition to $K_d$ values for leucettine 41 (Figure 2). These comprehensive screening approaches confirmed the rather good selectivity of each of the three studied compounds for DYRKs and CLKs and detected additional affinity for GSK-3, HIPK, IRAK1, CK2 (leucettine 41), or CK1 (harmine).

Altogether, our results confirmed that leucettine L41, harmine, and other inhibitors shared structure−activity relationship (SAR) regarding inhibition of CLK and DYRK kinases. Further chemistry work will be required to generate CLKs- and DYRKs-selective inhibitors from these scaffolds.

**Selectivity of Leucettine L41. (2) Affinity Chromatography Approaches.** We next made use of the Evotec/Kinaxo technology to investigate the targets of leucettine L41 in mouse brain. Briefly, the method is based on an affinity matrix comprising several well-characterized broad-spectrum kinase inhibitors to enrich the subproteome of endogenously expressed kinases of cells or tissues.[19] Kinase inhibitors are screened against these matrix-bound proteins to reveal the inhibitor's quantitative cellular target profile. First, a lysate of mouse brain was applied to the KinAffinity matrix comprising a mixture of various immobilized broad-band kinase inhibitors, adjusted to different concentrations. These quantitative binding experiments allow determination of the concentration of the immobilized compounds required to obtain 50% binding of each target protein to the matrix ($BC_{50}$). Second, a lysate of mouse brain was applied to the KinAffinity matrix with the highest loading density of kinase inhibitors in the presence of increasing concentrations of free leucettine L41. These quantitative competition experiments determine the free compound concentration required for 50% target protein to remain bound to the matrix ($CC_{50}$). The final $K_{d,free}$ values for the free compound were calculated for each target protein using the Cheng−Prusoff equation.[20] A total of 143 distinct protein kinases and five lipid kinases were enriched from mouse brain (Supporting Information Table S6A). Leucettine L41 targets were ranked according to their affinities with $K_d$ values ranging from 0.021 up to 15.265 μM (Table 2). A total of six target kinase proteins and two associated proteins were identified in mouse brain tissue for leucettine L41. These targets included SLK, DYRK1A, CK2 $\alpha$1 and $\alpha$2, and associated $\beta$ subunit, GSK-3$\alpha$, and the lipid kinase PIKfyve (phosphatidylinositol-3-phosphate 5-kinase) and its associated Vac14 protein (Table 2).

To further evaluate the scope and nature of targets binding to leucettine L41 in the context of complex tissue extracts, we used another affinity chromatography method that has been successfully exploited previously with other kinase inhibitors.[21] Leucettine L41 was covalently immobilized through a polyethylene linker on agarose beads (Burgy et al., unpublished) (Figure 3A). The position of the linker on the inhibitor was selected on the basis of the inhibitor's interactions and orientation in the DYRKs' and CLKs' ATP-binding sites, as revealed by kinase/inhibitor cocrystal structures[6] (see below). Extracts of immortalized mice hippocampal HT22 cells and mouse brains were exposed to the immobilized inhibitor matrix, the beads were extensively washed, and the bound proteins were analyzed by SDS-PAGE followed by Western blotting (Figure 3B,C). In cell as well as in tissue samples, the expected targets (DYRK1A, GSK-3 ($\alpha$, $\beta$1, and $\beta$2 isoforms), CK2 ($\alpha$, $\alpha'$, and $\beta$ subunits), and PIKfyve/Vac14/Fig4) were identified. No binding was observed on control ethanolamine beads devoid of ligand. Binding of all detected leucettine L41 targets on beads was abolished, at least partially, by addition of an excess of free leucettine L41 to the extracts (Figure 3B,C).

**Structural Insight into the Binding of Leucettine L41 with Its Kinase Targets.** To better understand these kinase/inhibitor selectivities and to generate models for structure based optimization, we cocrystallized leucettine L41 with DYRK1A, DYRK2, CLK3, and PIM1 (Figure 4). The cocrystal


dx.doi.org/10.1021/jm301034u | J. Med. Chem. 2012, 55, 9312−9330

Leucettamine B

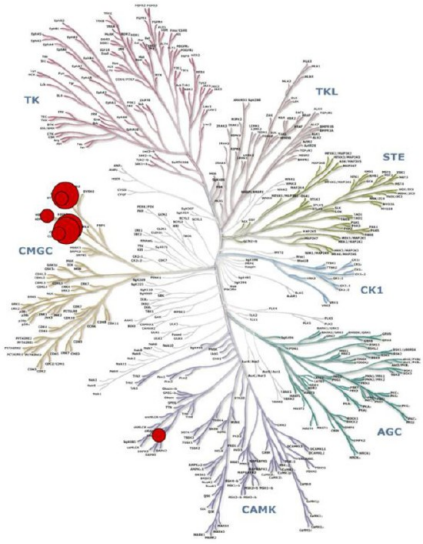


| Kinases | Score |
|---|---|
| DYRK1A | 1.6 |
| CLK1 | 2.2 |
| CLK4 | 2.6 |
| CLK2 | 10.0 |
| DYRK1B | 11.0 |

Leucettine L41

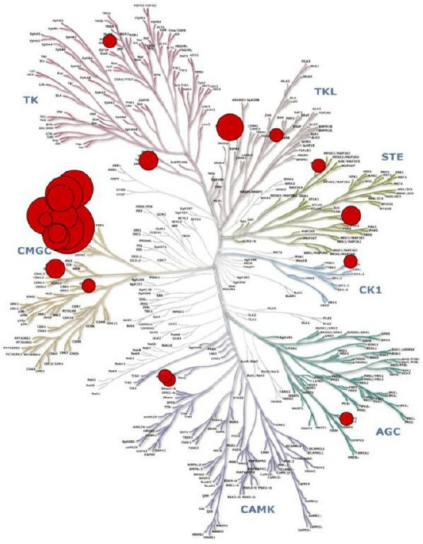


| Kinases | Score | Kd (nM) |
|---|---|---|
| CLK4 | 0 | 70.0 |
| DYRK1A | 0.20 | 7.8 |
| CLK1 | 0.25 | 75.0 |
| DYRK2 | 0.60 | 450.0 |
| HIPK1 | 0.75 | 320.0 |
| CLK3 | 2.0 | 1100.0 |
| IRAK1 | 2.8 | 930.0 |
| HIPK3 | 3.8 | 230.0 |
| DYRK1B | 4.0 | 140.0 |
| CLK2 | 5.6 | 360.0 |
| TAOK1 | 8.8 | 1700.0 |
| TYK2 * | 9.0 | n.t. |
| GSK3A | 9.8 | 550.0 |

Harmine

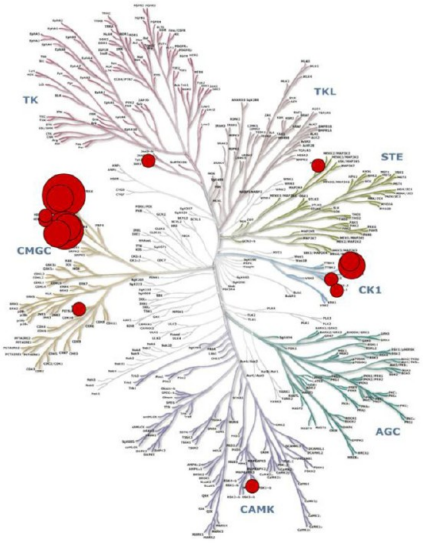


| Kinases | Score |
|---|---|
| DYRK1A | 0.1 |
| CLK1 | 0.35 |
| DYRK1B | 2.0 |
| CLK4 | 2.1 |
| CLK2 | 2.6 |
| CSNK1E | 2.8 |
| CSNK1D | 7.0 |
| CSNK1G2 | 10.0 |

**Figure 2.** Comparison of interaction of leucettamine B, leucettine L41, and harmine with 402 human kinases (KinomeScan). Compounds were tested at a 10 $\mu$M final concentration in the kinase interaction panel (402 kinases). A semiquantitative scoring of this primary screen was estimated. This score relates to a probability of a hit rather than strict affinity. Scores >10, between 1 and 10 and <1 indicate the probability of a being a false positive is <20%, < 10%, < 5%, respectively. Results are presented as TREEspot kinase interaction maps (top) and best selectivity scores (bottom). Actual $K_d$ were determined, in the case of leucettine L41, for all kinases displaying a score <10. *: JH2 domain-pseudokinase. Raw data (all 402 values) are provided in the Supporting Information Table S5.

**Table 2. Leucettine L41-Binding Proteins from Mouse Brain As Identified by Competition Affinity Chromatography (KinAffinity, by Kinaxo Biotechnologies, Evotec)[a]**

| | leucettine L41 interacting proteins | | |
|---|---|---|---|
| code | protein | synonym | $K_{d,free}$ [$\mu$M] |
| O54988 | STE20-like serine/threonine-protein kinase | SLK | 0.021 |
| Q61214 | dual specificity tyrosine phosphorylation regulated kinase 1A | DYRK1A | 0.065 |
| Q60737 | casein kinase 2 subunit $\alpha$ | CSNK2A1 | 0.326 |
| *P67871* | *casein kinase 2 subunit $\beta$* | *CSNK2N* | *0.382* |
| O54833 | casein kinase 2 subunit $\alpha$ | CSNK2A2 | 0.574 |
| Q2NL51 | glycogen synthase kinase-3 $\alpha$ | GSK3A | 3.274 |
| Q9Z1T6 | phosphatidylinositol-3-phosphate 5-kinase type III | PIKFYVE | 6.010 |
| *Q80WQ2* | *protein VAC14 homologue* | *VAC14* | *15.265* |

[a]Six kinases and two non-kinase proteins were identified as leucettine L41 targets ($K_d$ value <16 $\mu$M). Non-protein kinases are indicated in italics.

structure with CLK3 has been reported previously.[6] The structures for DYRK1A, DYRK2, and PIM1 were determined at 3.15, 2.55, and 2.00 Å resolutions, respectively (Supporting Information Table S7). The close derivative leucettine L4 was also cocrystallized with GSK-3$\beta$ (Supporting Information Table S8), and from this structure we generated a model of the leucettine L41/GSK-3$\beta$ complex (Supporting Information Figure S1).

As expected, leucettine L41 binds in the ATP binding pocket of all kinase targets that were cocrystallized (Figure 4), acting as an ATP competitive inhibitor. In DYRK1A and DYRK2, leucettine L41 forms two direct polar interactions (Figure 4B,C). One hydrogen bond is formed to the hinge backbone amide of Leu241 (residue numbers refer to DYRK1A) and another from the 2-aminoimidazolone carbonyl to conserved active site lysine (Lys188). In addition, there are three hydrogen-bonding interactions mediated by water molecules. These water molecules can be seen in the DYRK2 data (Figure 4C), and although the lower resolution of the DYRK1A data precludes including water molecules in the model, there is nevertheless weak positive difference electron density to support the presence of a similar hydrogen bonding network


dx.doi.org/10.1021/jm301034u | J. Med. Chem. 2012, 55, 9312−9330

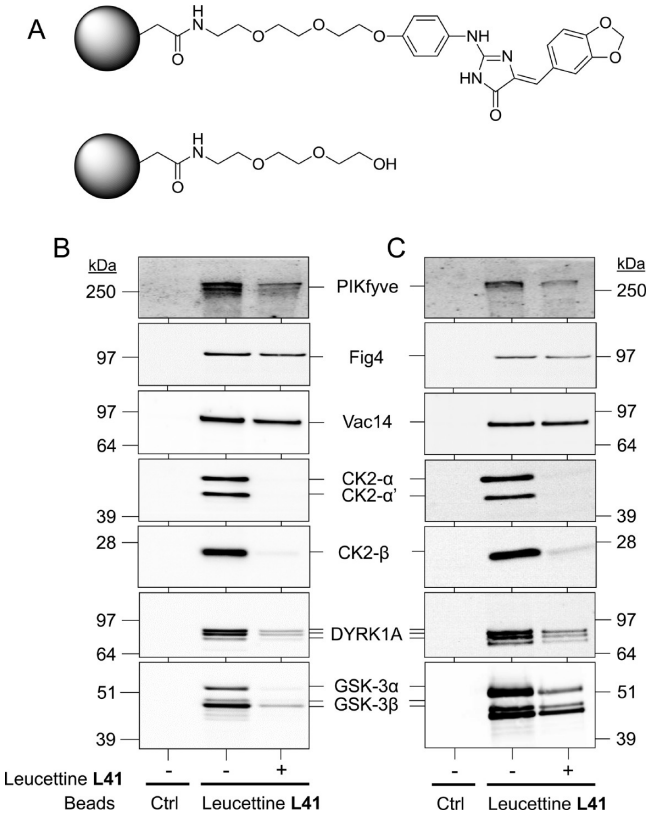


**Figure 3.** Affinity chromatography on immobilized leucettine L41 reveals kinase targets. (A) Leucettine L41 was immobilized through a polyethylene linker to agarose beads. Control beads were made with a polyethylene linker without ligand. (B,C) Extracts of immortalized mice hippocampal cells (HT22) (B) or mouse brain (C) were loaded on control beads (Ctrl) or leucettine L41-beads in the absence (−) or presence (+) of free leucettine L41. After extensive washing of the beads, the bound proteins were resolved by SDS-PAGE and were detected by Western blotting with antibodies directed against GSK-3$\alpha/\beta$, DYRK1A, CK2 $\alpha/\alpha'$, CK2 $\beta$, Vac14, Fig4, and PIKfyve.

in DYRK1A as in DYRK2. This hydrogen bonding network involves Lys188, the carboxyl group and backbone nitrogen of the DFG motif aspartate (Asp307), and the amide of Asn292 (Figure 4B,C). In addition, leucettine L41 forms several hydrophobic contacts involving Leu294, Val222, Leu241, and Val306. The ATP binding site of DYRK2 is highly similar to that of DYRK1A with just three nonconserved residues. DYRK1A Val222 is an isoleucine in DYRK2, while the DYRK1A hinge residue Met240 is a leucine in DYRK2 which slightly decreases hydrophobicity and opens the pocket. However, these residue differences do not seem pivotal for DYRK1A/leucettine L41 specificity. The third residue difference appears to be the most important. The residue that precedes the DFG motive is an isoleucine in DYRK2 (Ile294) and a valine (Val306) in DYRK1A, resulting in significant changes in hydrophobic contact surface. In CLK3, an alanine occupies this position, drastically reducing interaction with leucettine L41 and explaining the significantly weaker potency of leucettine L41 for this kinase (DYRK1A 0.040 $\mu$M; CLK3 >10 $\mu$M) and higher affinity for other CLKs that contain large hydrophobic residues at this position. Leucettine L41 assumes a similar binding mode in all three complexes. Supporting Information Figure S3 shows the differences in hydrophobic inhibitor binding interactions at the back of the binding pocket between DYRK2, DYRK1A, and CLK3.

Our cross-screening unexpectedly identified PIM1 as a potential target for leucettine L41 with a moderate $IC_{50}$ of 0.88 $\mu$M. PIM1 shares little homology with DYRKs and CLKs, and we were interested to see if leucettine L41 binds to this diverse ATP binding site in a similar way, and so we cocrystallized leucettine L41 with PIM1 to investigate this issue (Supporting Information Figure S3). Most likely as a result of the weak activity of leucettine L41 for PIM1, we observed two alternative binding modes, with potentially further binding modes that were not modeled. The main binding mode (modeled with 70% occupancy) showed a similar inhibitor orientation as observed in DYRK/CLK. However, despite conservation of its orientation, leucettine L41 forms very different interactions with PIM1. First, the insertion of a proline reside in the hinge region abolishes the possibility of forming a hinge backbone hydrogen bond as observed in DYRK/ and CLK/leucettine L41 complexes. Second, the 2-aminoimidazolone interacts differently with the PIM1 back pocket by forming two hydrogen bonds with the DFG aspartate (Asp186) as well as to a conserved water molecule. In the second orientation, leucettine L41 flips 180° in the PIM1 ATP binding site. As a result, Asp307 also reorients pointing away from the inhibitor (Supporting Information Figure S4).

To elucidate leucettine L41 interaction with GSK-3$\beta$, we also made a docking model based on a cocrystal with the previously reported leucettine L4[6] (Supporting Information Figure S1). Docking resulted in a structure related to the DYRK cocrystal structures, a similar hydrogen bond network, and similar orientation of this inhibitor. The lower affinity of leucettine L41 for GSK-3 may be due to the different hydrophobic pocket as observed for CLK3 because Val306 in DYRK1A is replaced by a cysteine, but this point cannot be demonstrated with our present docking model.

The most conserved feature between all these inhibitors is the hydrogen receptor in front of Leu241 amine which is also involved in ATP binding. Highly potent inhibitors such as harmine (Supporting Information Figure S2A)[15] and INDY (Supporting Information Figure S2B)[22] have a common interaction with DYRK. All inhibitors share a six- or seven-membered aromatic ring which binds into the hydrophobic pocket. This allows strong dispersion interactions with the protein. 7-Bromo-, 3′-oxime, 5′-carboxy-indirubin (Supporting Information Figure S2C), related to the GSK3 inhibitor 6-bromo-, 3′-oxime-indirubin (6BIO),[23] has four hydrogen bonds but a lesser hydrophobic scaffold because of a pyrrole ring substituting the canonical benzyl ring. The $IC_{50}$ of indirubins is about 50 times higher than that of leucettine L41. Their lower potency supports our hypothesis that strong apolar interactions are pivotal for good DYRK1A inhibition. In addition of these common features, inhibitors usually interact with the phosphate binding groove, deeper in the pocket. This region contains several polar groups such as arginine or aspartate and consequently can easily create hydrogen bonds with small molecules. These links seem to be responsible for the small differences in $IC_{50}$ values between strong inhibitors. Within the inhibitors we compared, the two best affinities are with leucettine L41 and debromohymenialdisine. They form more H-bonds than other inhibitors and possess a highly hydrophobic scaffold. KH−CB19 has a different means of interacting with the catalytic groove (Supporting Information Figure S2E). It makes a hydrogen bond with Glu239 in the hinge.[24] Its


dx.doi.org/10.1021/jm301034u | J. Med. Chem. 2012, 55, 9312−9330

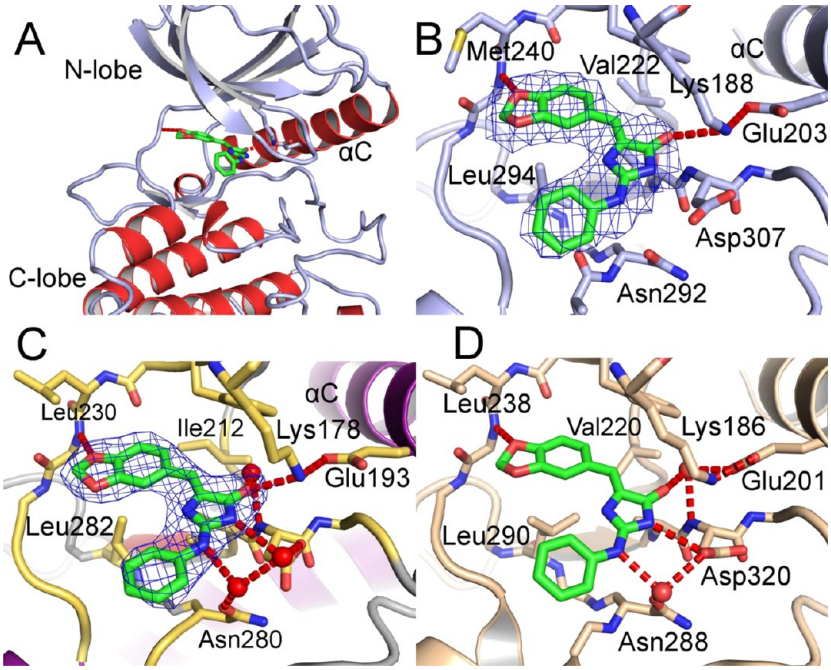


**Figure 4.** Co-crystal structures of leucettine L41 with DYRK1A, DYRK2, and CLK3. (A) General view of DYRK1A/leucettine L41 cocrystal in ribbon representation. (B) Active site view of DYRK1A/leucettine L41. The $2F_o - F_c$ electron density map contoured at 1.0 $\sigma$ around leucettine L41 is shown in blue. (C) Active site view of DYRK2/leucettine L41. The $2F_o - F_c$ electron density map contoured at 1.0 $\sigma$ around leucettine L41 is shown in blue. (D) Active site view of CLK3/leucettine L41 from the same orientation as (B) and (C). Figures were prepared using Pymol (www.pymol.org).

benzyl ring is displaced by roughly 1 Å compared to leucettine L41 but still remains in the hydrophobic pocket. It also links Glu292 and Asn293 in the conserved sequence DLKPENILL under the groove. These two H-bonds attract the inhibitor in a lower and unusual position. Even though the great majority of DYRK inhibitors show very similar interactions with the kinase, other dockings are still possible and need to be further explored.

**Inhibition of Endogenous Kinase Targets in Cells by Leucettine L41.** To confirm the effects of leucettine L41 on endogenous cellular kinases in vivo, we used HT22 cells. Cells were exposed for 4 h to increasing concentrations of leucettine L41 and collected for analysis of their DYRK1A and GSK-3 expression and activity levels. Exposure to the inhibitor did not modify the expression of both kinases as shown by Western blotting analysis of total extracts with appropriate antibodies (Figure 5A,B). Native GSK-3 and DYRK1A were purified, by affinity chromatography on axin beads[25] and immunoprecipitation, respectively, from HT22 cells exposed to various leucettine L41 concentrations and these kinases were assayed with appropriate substrates. Results showed that although endogenous GSK-3 activity remained constant, DYRK1A activity was dose-dependently inhibited (Figure 5C). As an alternative way to assess endogenous GSK-3 activity, the phosphorylation of one of its substrates, $\beta$-catenin, was evaluated using phospho-$\beta$-catenin specific antibodies. Because phosphorylation of $\beta$-catenin leads to its proteolytic degradation, we also made use of a proteasome inhibitor, MG132,[26] to enhance the phospho-$\beta$-catenin signal. HT22 cells were exposed for 24 h to various concentrations of leucettine L41, or 10 $\mu$M of two reference GSK-3 inhibitors, 6BIO[23] and alsterpaullone,[27] in the presence or absence of 10 $\mu$M MG132. Proteins were extracted and resolved by SDS-PAGE, and phospho-$\beta$-catenin was detected by Western blotting. Results show that, as expected, MG132 greatly enhanced the phospho-$\beta$-catenin level (Figure 5D). As also expected, 6BIO and alsterpaullone strongly reduced the phospho-$\beta$-catenin level. In contrast, leucettine L41 did not alter this pathway, further supporting the idea that, although it may interact with GSK-3 in vitro (purified kinases, cell extracts), it does not inhibit GSK-3 activity in cell cultures (Figure 5D). Although DYRK1A binding to the leucettine L41 matrix was competed by free leucettine L41 added to HT22 cell extracts but not by free alsterpaullone, both compounds prevented binding of GSK-3 to the leucettine L41 matrix (Figure 5E). These experiments suggest that leucettine L41 interacts directly and independently with DYRK1A and GSK-3. When HT22 cells were treated for 4 h with either 10 $\mu$M leucettine L41, 10 $\mu$M alsterpaullone, or both, only endogenous DYRK1A, but not endogenous GSK-3, was inhibited by leucettine L41, while alsterpaullone inhibited GSK-3 but not DYRK1A (Figure 5F). These results confirm that leucettine L41, although it may interact with GSK-3 in vitro, does not seem to inhibit GSK-3 in a cellular context.

Inhibition of endogenous CLKs was assayed in an indirect fashion. Indeed it is known that CLK1 pre-mRNA splicing is under control of the catalytic activity of CLK1.[17,28] We have shown previously that leucettine L41 prevents alternative splicing of a CLK1 minigene construct, mimicking the effect of a kinase dead CLK1 mutant.[6] We confirmed these results with endogenous CLK1 and CLK4 (Figure 6). HT22 cells were exposed for 6 h to increasing concentrations of leucettine L41 and mRNAs were extracted, purified, and reverse-transcribed. Appropriate primers were used to detect the two main splice variants of CLK1 and CLK4. A dose-dependent inclusion of CLK1 and CLK4 exon 4 was detected (Figure 6), suggesting that leucettine L41 inhibits endogenous CLK1 and CLK4, thereby affecting alternative splicing of CLK1 and CLK4 pre-mRNAs and presumably of other pre-mRNAs.


dx.doi.org/10.1021/jm301034u | J. Med. Chem. 2012, 55, 9312−9330

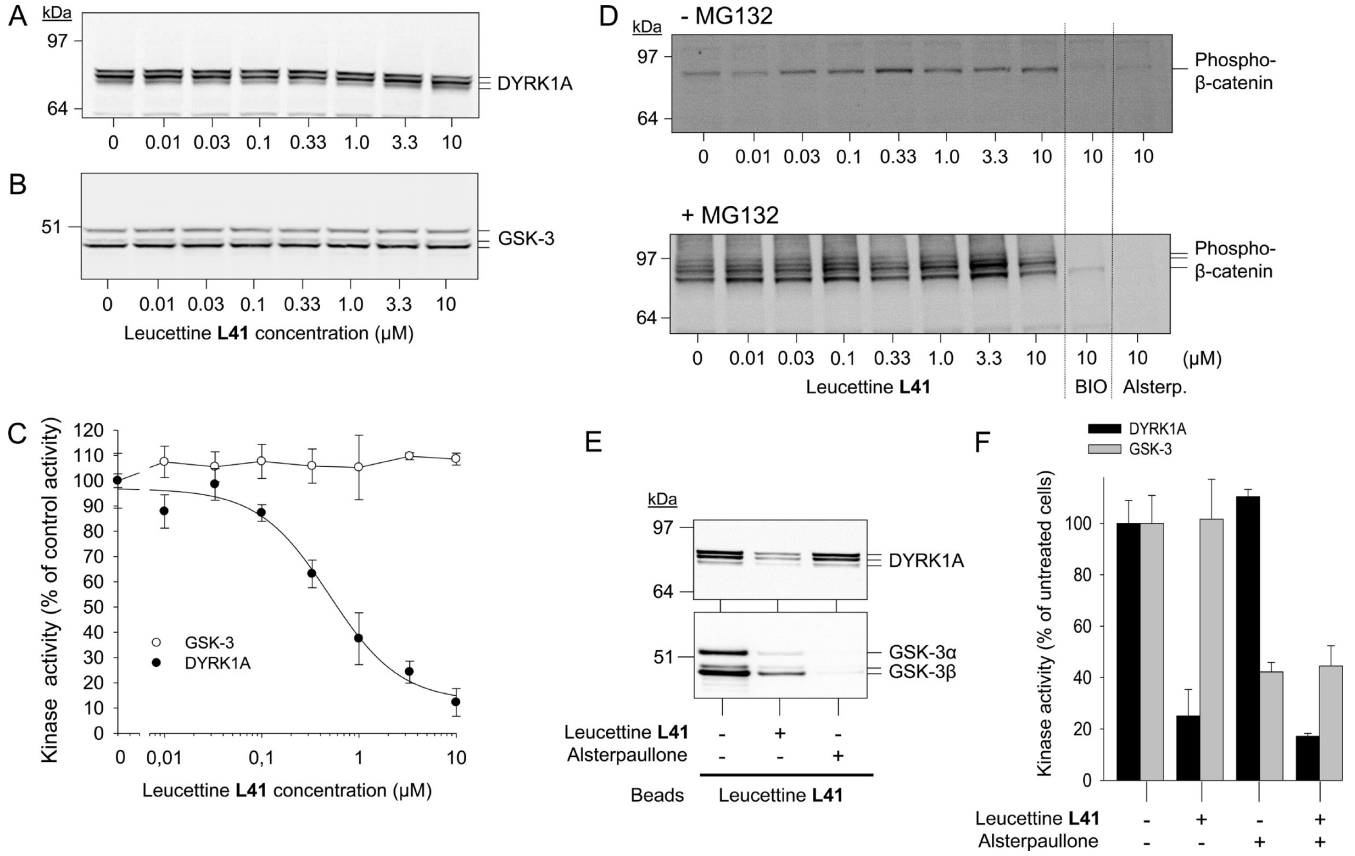


**Figure 5.** Leucettine L41 inhibits endogenous DYRK1A activity in cell cultures but not GSK-3. HT22 cells were exposed to increasing concentrations of leucettine L41 for 4 h. Cells were then pelleted, frozen, and extracted. Expression levels of DYRK1A (A) and GSK-3 (B) were estimated by Western blotting following SDS-PAGE. (C) Catalytic activities were assayed with appropriate substrates, following immunoprecipitation with appropriate antibodies (DYRK1A) or affinity purification with axin−agarose (GSK-3). Activities are expressed relative to the kinase activities present in control, vehicle-treated cells. (D) HT22 cells were treated or not with 10 $\mu$M MG132, immediately followed by leucettine L41, 6BIO, or alsterpaullone at the indicated concentrations. Phospho-$\beta$-catenin levels were estimated by Western blotting. (E) Extracts of immortalized mice hippocampal cells (HT22) were loaded on control beads or leucettine L41 beads in the absence (−) or presence (+) of free leucettine L41 or alsterpaullone. After extensive washing of the beads, the bound proteins were resolved by SDS-PAGE and were detected by Western blotting with antibodies directed against DYRK1A or GSK-3. (F) Effects of leucettine L41 and alsterpaullone on endogenous HT22 DYRK1A and GSK-3 kinase activity. HT22 cells were exposed or not to 10 $\mu$M leucettine L41, 10 $\mu$M alsterpaullone, or both, for 4 h. Cells were then pelleted, frozen, and extracted. Their DYRK1A and GSK-3 kinases were purified and catalytic activities were assayed with appropriate substrates. Activity is expressed relative to the kinase activities present in control, vehicle-treated cells.

**Leucettine L41 Provides Protection against Glutamate-Induced Cell Death.** Glutamate-mediated excitotoxicity contributes to neuronal cell death associated with both acute and chronic central nervous system diseases. We have thus used this cell death inducer and hippocampal HT22 cells to evaluate the neuroprotective properties of leucettine L41. HT22 cells were exposed to increasing concentrations of glutamate. Cell death was induced in a dose-dependent manner ($IC_{50}$ 2 mM) (Figure 7A). When cells were simultaneously treated with various doses of leucettine L41, a dose-dependent protection against glutamate-induced cell death was observed (Figure 7A). This effect was observed to a lower extent with alsterpaullone, while the PIKfyve inhibitor YM-201636[29] and the CK2 inhibitor CX-4945[30] had no protective effects against glutamate-induced HT22 cell death (data not shown). These results suggest that inhibition of PIKfyve and CK2 is unlikely to contribute to the neuroprotective effects of leucettine L41 and that inhibition of DYRKs, CLKs or unidentified targets prevents neuronal cell death induced by glutamate. A kinetics study showed that leucettine L41 mediated neuroprotection was stable even up to 48 h after glutamate addition (Figure 7B).

**Leucettine L41 Reduces Neurodegeneration in Amyloid Precursor Protein Transfected Brain Slices.** To evaluate the physiological effect of DYRK1A inhibition in the context of amyloid precursor protein (APP) induced neurodegeneration, we took advantage of a previously developed brain slice assay platform.[31] The fate of neurons is highly dependent on the complex tissue environment in which they are resident, thus maintaining the cellular architecture of brain tissue as intact as possible is essential for a functional assay. Particle-mediated gene transfer of APP or mutant huntingtin protein can induce progressive neurodegeneration in a corticostriatal brain slice model.[31] We thus used an acute APP challenge model to evaluate the role of the DYRK1A in neurodegeneration in cortical pyramidal neurons. In particle mediated gene transfer, gold particles are coated with DNA encoding proteins of interest and introduced into acutely prepared brain slices using a "gene gun". Expression of the proteins of interest is typically seen within 24 h in transfected neurons throughout the transfected slice.

To determine the importance of DYRK1A in APP-induced neurodegeneration, cortical brain slices were transfected with


dx.doi.org/10.1021/jm301034u | J. Med. Chem. 2012, 55, 9312−9330

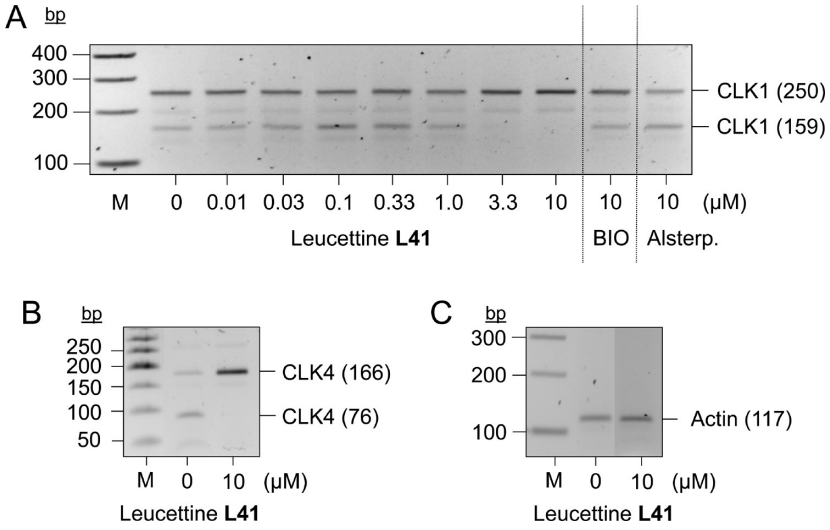


**Figure 6.** Leucettine L41 inhibits CLK1 and CLK4 alternative splicing. (A) HT22 cells were exposed to increasing concentrations of leucettine L41 for 6 h. Cells were then pelleted and snap frozen. Total mRNA was extracted and reverse-transcribed. CLK1 with or without exon 4 (250 or 159 bp fragment, respectively) was then amplified by PCR, and the reaction products were resolved by electrophoresis on agarose. (B) CLK4 with or without exon 4 (166 or 76 bp fragment, respectively) was also amplified. (C) Expression of actin mRNA (117 bp fragment) was used as an internal control.

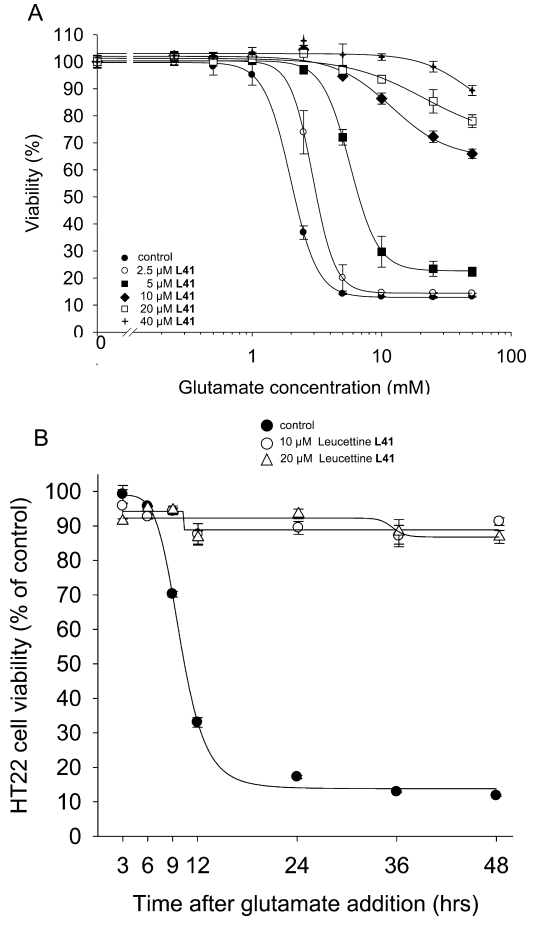


**Figure 7.** Leucettine L41 protects HT22 cells from glutamate-induced cell death. (A) HT22 cells were exposed to increasing concentrations of glutamate for 24 h in the presence of 0–40 $\mu$M leucettine L41 and their viability was assessed by the MTS assay. (B) Time-dependence of glutamate-induced cell death and protection by 10 or 20 $\mu$M leucettine L41.

APP and incubated in the presence of varying doses of leucettine L41, harmine, or vehicle control. We found that leucettine L41 caused a dose-dependent inhibition of the neurodegeneration induced by APP (Figures 8A,C). Leucettine L41 seemed not to affect brain slice health, positively or negatively, when added to control slices transfected only with EYFP for visualization. The same experiment was repeated in the presence of varying doses of harmine, and a similar but somewhat more modest reduction of neurodegeneration was seen when high concentrations of harmine were used (Figure 8B). Finally, we inhibited endogenous DYRK1A expression in untreated cortical brain slice explants using a pool of siRNAs delivered together with APP on the same biolistic gold particles. We found that such knockdown of DYRK1A by RNA interference inhibited neurodegeneration induced by APP, whereas scrambled siRNA did not (Figures 8D,E). Together, these experiments suggest that pharmacological or genetic inhibition of DYRK1A function may be a novel approach to reduce neurodegeneration caused in AD or in the context of Down syndrome where DYRK1A is expressed at elevated levels in the brain.

## ■ DISCUSSION

In this article we report an extensive analysis of the selectivity of leucettine L41, a representative member of the leucettines family of kinase inhibitors derived from the marine natural product leucettamine B. We also describe the molecular interactions of leucettine L41 with its targets and its neuroprotective properties.

**Pharmacological Inhibitors of DYRKs and CLKs.** A rapid screen of reference kinase inhibitors (Supporting Information Tables S1 and S2) showed that many previously known scaffolds (purines, indirubins, meriolins, flavones, etc..) display some inhibitory activity toward DYRKs and CLKs, suggesting that selective inhibitors might be derived from these structures. This screen also revealed that most DYRKs inhibitors also inhibit CLKs and that reported DYRK1A-specific and CLK-specific reference inhibitors (Harmine and TG003, respectively) were in fact dual-specificity inhibitors of


dx.doi.org/10.1021/jm301034u | J. Med. Chem. 2012, 55, 9312–9330

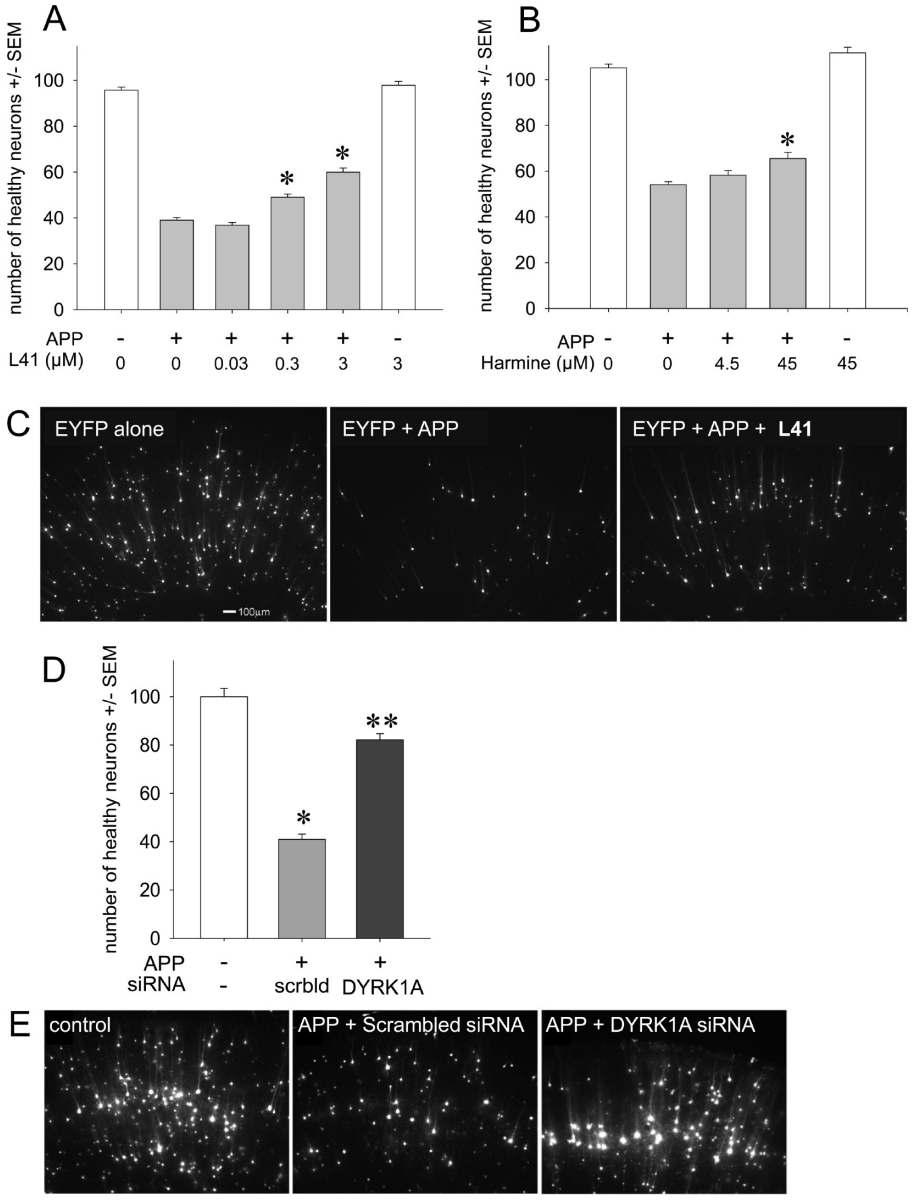


**Figure 8.** DYRK1A inhibition reduces neurodegeneration in APP transfected brain slices. (A) Rat brain slices were transfected with EYFP or EYFP and APP. The culture medium was supplemented with varying doses of leucettine L41. After 3 days, neuronal health was assessed in the cortex. APP in the presence of vehicle control induced significant neurodegeneration, which was significantly reduced by leucettine L41 in a dose-dependent manner. Leucettine L41 had no significant effect on neurons that were transfected with EYFP only. Asterisk indicates a statistically significant change at the confidence level $p < 0.05$ (ANOVA followed by Dunnett's post hoc comparison test). (B) A similar experiment was carried out with varying doses of harmine, which reduced neurodegeneration to a modest but significant degree. (C) Representative fluorescence microscope images depicting comparable cortical areas in brain slices in the presence or absence of leucettine L41. See Experimental Procedures for details of the quantification process. Images of live brain slices were taken at 40× magnification with a Zeiss SteREO Lumar fluorescence stereomicroscope equipped with a digital camera. (D) Rat brain slices were transfected with (i) EYFP, (ii) EYFP/APP/scrambled siRNA, or (iii) EYFP/APP/siRNA targeting DYRK1A. Neuronal health was assessed in the cortex after 3 days. APP in the presence of scrambled siRNA induced significant neurodegeneration, which was significantly reduced by siRNA targeting DYRK1A. Asterisk indicates a statistically significant difference between condition (i) and (ii): two asterisks indicates a statistically significant difference between conditions (ii) and (iii) (confidence level $p < 0.05$ by ANOVA followed by Dunnett's post hoc comparison test)). (E) Representative fluorescence microscope images for the summary data shown in (D) depicting comparable cortical areas in the brain slice explants.

both DYRKs and CLKs. This has been confirmed with leucettines. At this stage, no DYRK-specific or CLK-specific inhibitors have been reported yet, but we are starting to generate such compounds and investigating the molecular basis of their unique selectivity (unpublished data).

**Target Selectivity of Leucettine L41.** We have used four different methods to investigate the scope of leucettine L41's targets: activity and interaction assays of recombinant kinases, affinity chromatography on immobilized ligand, and competition affinity chromatography. These different methods confirmed that leucettine L41 targets the families of DYRKs and CLKs. They showed that the inhibitor also interacted with GSK-3, CK2, SLK, and the lipid kinase PIKfyve. These kinases are expressed to different levels in different tissues, and leucettine L41 action may thus be different in different tissues.


dx.doi.org/10.1021/jm301034u | J. Med. Chem. 2012, 55, 9312−9330

Interaction of leucettine L41 with DYRK1A, and other DYRKs, was consistently observed in all selectivity studies. DYRK1A inhibition by leucettine L41 was demonstrated in vitro (kinase assays, kinase interaction assay, affinity chromatography, cocrystallization) but also in vivo, as HT22 cells exposed to the inhibitor showed reduced endogenous DYRK1A activity. Although CLK inhibition was clearly demonstrated in vitro (kinase assays, kinase interaction assay, cocrystallization), its in vivo inhibition was shown only indirectly (due to the lack of availability of immunoprecipitating antibodies) by the alternative splicing (exon 4 inclusion) which results from CLK inhibition (Figure 6). Interaction with CK2 was revealed by the affinity chromatography competition assay and confirmed by direct in vitro kinase activity assays and affinity chromatography on immobilized leucettine L41. However, it was not detected earlier, especially in the Kinomescan approach, probably because this method used recombinant CK2 $\alpha$ catalytic subunits, whereas the affinity chromatography methods addressed the heterotetrameric holoenzyme (comprising the $\alpha$, $\alpha'$, and $\beta$ subunits) as shown by copurification of the $\beta$ subunit with the catalytic $\alpha$ and $\alpha'$ subunits during the two affinity chromatography experiments (immobilized leucettine, kinobeads). This native complex may have stronger interaction with leucettine L41 than recombinant catalytic subunits. We now need to confirm CK2 inhibition in vivo using antibodies against its phosphosubstrates. GSK-3 (preferentially GSK-3$\alpha$) was found as a leucettine L41 target in vitro (kinase assays, kinase interaction assay, affinity chromatography, cocrystallization). Surprisingly, although leucettine L41 inhibited GSK-3 in vitro, we were unable to see any in vivo GSK-3 inhibition in cultured cells exposed to the compound, although the well characterized GSK-3 inhibitors alsterpaullone and 6BIO inhibited GSK-3 in vivo (Figure 5). This may be due to the inclusion of GSK-3 in large protein complexes that prevent interaction with leucettine L41 in cell culture. Alternatively, intracellular distribution of leucettine L41 may not coincide with intracellular distribution of GSK-3, and leucettine L41 may bind to DYRKs, CLKs, and CK2 before it has a chance to encounter GSK-3. Another possibility is that leucettine L41, in contrast to alsterpaullone and 6BIO, preferentially binds to a kinase inactive GSK-3 pool and much less to the kinase active GSK-3 pool. We are currently investigating this possibility. Despites its lack of effect in cell culture, it remains possible that leucettine L41 inhibits GSK-3 in animal models. Due to the unavailability of good SLK antibodies, we were unable to confirm the effects of leucettine L41 on SLK in the cellular context. Leucettine L41 had only modest effect on the catalytic activity of recombinant SLK (66% residual activity in the presence of 10 $\mu$M leucettine L41). Finally, the interaction of PIKfyve with leucettine L41, initially detected with the affinity chromatography competition assay, was confirmed by Western blotting on the leucettine L41 sepharose beads (Figure 3 B,C). PIKfyve is a lipid kinase that catalyzes the phosphorylation of phosphatidylinositol-3-phosphate (PIP3P) to phosphatidylinositol-3,5-bisphosphate (PI(3,5)$P_2$). PI(3,5)$P_2$ levels are regulated by a protein complex comprising the scaffolding protein Vac14 (also known as ArPIKfyve), the lipid kinase PIKfyve (Fab1), the PIKfyve activator Vac7, the PIKfyve inhibitor Atg18, and the lipid phosphatase Fig4 (Sac3).[32] The copurification of Vac14, Fig4, and PIKfyve on the affinity chromatography matrices used here (Figure 3, Table 2) suggests that leucettine L41 interacted with the heteropentameric complex. Although it is more likely that leucettine L41 binds directly to PIKfyve, the possibility that it interacts physically with other members of the complex remains open. This point is currently under investigation.

**Neuroprotective Effects of Leucettine L41.** It is always difficult to attribute a biological effect of a compound to its interaction with a specific target when, like leucettine L41, it is able to interact with several kinases. It is therefore quite likely that the neuroprotective effects of leucettine L41 can be accounted for by the cooperative inhibition of several targets. As discussed below, many of the known leucettines targets are correlated with the development of AD and other neurodegenerative diseases.

There are several arguments that link DYRK1A with AD: (1) DYRK1A phosphorylates key AD proteins Tau,[33] APP,[34] presenilin,[35] septine-4,[36] RCAN,[37] and Munc18−1.[38] (2) DYRK1A acts as a "priming" kinase for GSK-3. It phosphorylates Tau on Thr212, which can then be phosphorylated by GSK-3 on Ser208.[33a] GSK-3 is a major player in AD (see below). (3) Genetic studies have directly linked DYRK1A with the onset and development of AD.[39] (4) The DYRK1A gene is located on chromosome 21. Overexpression of DYRK1A is associated with early AD phenotype in all Down syndrome patients.[40] (5) DYRK1A is involved regulating pre-mRNA splicing, and there are some splicing events, such as the alternative splicing of Tau[41] (see below), that are associated with AD. Altogether these results confirm that inhibition of DYRK1A activity is a valid approach in the development of anti-AD therapeutic drugs.

There is less evidence for CLKs as potential targets in AD. CLK2 is a key regulator of Tau exon 10 alternative splicing.[42] There is growing evidence for modified alternative splicing in AD,[43] and splicing regulating kinases such as CLKs may thus turn out to be appropriate therapeutic targets.

There is very solid evidence for the involvement of GSK-3 in AD and the therapeutic potential of pharmacological inhibitors of GSK-3 in AD (review in ref 44). GSK-3 thus constitutes a valid inhibition target, and already one GSK-3 specific inhibitor, tideglusib, has been brought in clinical trials against AD.[45]

There is only limited information available on potential links between CK2 and AD.[46] CK2 (and $Ca^{2+}$/calmodulin-dependent kinase) mediates both amyloid $\beta$ oligomers induced loss of insulin receptors and *N*-methyl-D-aspartate (NMDA) glutamate receptors[46a] and fast axonal transport inhibition.[46b] Pharmacological inhibition of CK2 may thus constitute another promising AD therapeutic approach.

The unexpected interaction of leucettine L41 with PIKfyve/Vac14/Fig4 opens several questions. Which protein, among the five subunits of the complex (Vac14, PIKfyve, Vac7, Atg18, Fig4), does directly bind leucettine L41, indirectly allowing the copurification of the other four partners by affinity chromatography? Interfering with the PIKfyve complex activity is expected to modify the PI(3,5)$P_2$/PIP3P ratio one way or the other, but at this stage we do not know in which direction leucettine L41 is acting. What is the link between interaction of leucettine L41 with the PIKfyve complex and its neuroprotective effects? There are several links between PIKfyve complex and neurodegeneration:[47,48] (1) PIKfyve regulates degradation of the voltage-gated Cav1.2 channel and prevents excitotoxic cell death.[47a] PIKfyve knockdown increases neuronal susceptibility to exicitoxicity. (2) Loss of Vac14 in a mouse mutant results in defective membrane trafficking pathways (endosome to trans-Golgi network) and massive neurodegeneration.[47b] A missense mutation of Vac14, preventing interaction with PIKfyve, was


dx.doi.org/10.1021/jm301034u | J. Med. Chem. 2012, 55, 9312−9330

described in a spontaneous neurological mouse mutant with autosomal recessive inheritance (infantile gliosis).[32e] (3) Mutations in PIKfyve are associated with François−Neetens fleck corneal dystrophy.[47c] (4) Loss of function of the Fig4 gene in a spontaneous mouse mutant (pale tremor)[48] causes neurodegeneration. Mutations in human Fig4 lead in inability to interact with Vac4, resulting in the peripheral nerve disorder Charcot−Marie−Tooth syndrome (CMT4J).[48]

## CONCLUSION

At this stage, it is impossible to attribute the observed neuroprotective effects of leucettine L41 to a specific interaction with a defined kinase target. Targets other than protein kinases have not been ruled out. It is quite likely that combined interactions of leucettines with several relevant targets provide the final neuroprotection observed in various models. It is also quite likely that the molecular mechanisms may be different in the different models used so far, namely glutamate-induced excitotoxicity in cell culture, brain slices in culture, or intracerebroventricular injected amyloid $\beta$25−35 peptide in mouse (T. Maurice et al., unpublished results).

Altogether, the results presented here show that leucettines, as exemplified by leucettine L41, target a subset of protein and lipid kinases involved in neurodegenerative pathology and display neuroprotective effects in early biological models. They constitute a promising family of pharmacological inhibitors for the development of novel AD therapeutic agents.

## EXPERIMENTAL PROCEDURES

**Chemicals and Reagents.** *Synthesis of Leucettamine B, Leucettines L41 and L4, and Immobilized Leucettine L41.* The products leucettamine B or (5*Z*) 2-amino-5-[(1,3-benzodioxol-5-yl)methylene]-3-methyl-3,5-dihydro-4*H*-imidazol-4-one, leucettine L41 or (5*Z*) 5-(1,3-benzodioxol-5-yl)methylene-2-phenylamino-3,5-dihydro-4*H*-imidazol-4-one, and leucettine L4 or (5*Z*) 5-[(1,3-benzodioxol-5-yl)methylene]-3-methyl-2-isopropylamino-3,5-dihydro-4*H*-imidazol-4-one were synthesized according to our previously described method.[6]

The strategy used for the synthesis of immobilized leucettine L41 through a polyethylene glycol linker (for affinity chromatography on agarose beads) is outlined in Supporting Information Scheme 1 and fully described in the Supporting Information. Purity of the products was controlled by DAD UV/vis 200−360 nm detector. Purity was further monitored by high resolution mass spectrometry (HRMS). The HRMS mass spectra were taken on a MS/MS ZABSpec Tof Micromass (EBE TOF geometry) at an ionizing potential of 8 eV. Purity of the final products was 95−97%.

*Other Reagents.* The following kinase inhibitors were obtained from our collaborators: olomoucine, (*R*)-roscovitine, and (*S*)-CR8 (N. Oumata and H. Galons), purvalanol A (N. Gray), 6BIO and other indirubins (L. Skaltsounis), aloisine A (G. Mettey), hymenialdisine (G.R. Pettit), kenpaullone and alsterpaullone (C. Kunick), variolin B and meriolins (B. Joseph), CX-4945 (C. Cochet), and TG003 (M. Hagiwara). Adenosine triphosphate (ATP), CNBr-activated sepharose 4B, dithiothreitol (DTT), donepezil, fisetin, flavopiridol, galantamine, Gleevec, glutamate, $\beta$-glycerophosphate, harmine, histone H1 (type III−S), IC261, IPTG (isopropyl-$\beta$-D-thiogalactopyranoside), luteolin, memantine, MG-132, Mops, *p*-nitrophenylphosphate, phenylphosphate, rivastigmine, sodium vanadate, staurosporine, tacrine, UO126 were obtained from Sigma Chemicals. YM-201636 was purchased from Symansis (New Zealand). The L'Oréal compound was synthesized as described in the Supporting Information. The GSK-3, CK1, DYRKs, and CLKs peptide substrates were obtained from Proteogenix (Oberhausbergen, France).

**Crystallography.** *Cloning, Protein Expression, and Purification.* PIM1 protein was purified as previously described.[49] Human GSK-3$\beta$−axin (383−401) complex was prepared as previously described.[50]

DNA for DYRK1A 127−485 or DYRK2 74−479 was PCR amplified from cDNA and inserted into expression vector pNIC28-Bsa4 by ligation independent cloning. The expression vector added an N-terminal hexahistidine tag and a TEV (tobacco etch virus) protease tag cleavage site to the expressed proteins. The plasmids were transformed into chemically competent *Escherichia coli* BL21(DE3)-R3-pRARE2 cells (phage-resistant derivative of BL21(DE3) with a pRARE2 plasmid) which were grown overnight at 37 °C in Luria−Bertani medium (LB-broth) containing 50 $\mu$g/mL kanamycin and 34 $\mu$g/mL chloramphenicol. These cultures were used to inoculate 1 L volumes of LB-broth containing 50 $\mu$g/mL kanamycin in 2 L baffled shaker flasks, which were allowed to grow at 37 °C to an optical density (OD600) of about 0.5 before the temperature was decreased to 18 °C. Protein expression was induced overnight at 18 °C with 0.1 mM IPTG. The bacteria were harvested by centrifugation and were frozen at −20 °C. Cells were resuspended in lysis buffer (50 mM HEPES pH 7.5 at 25 °C, 500 mM NaCl, 5 mM imidazole, 5% glycerol, 0.5 mM TCEP) in the presence of protease inhibitor cocktail (1 $\mu$L/mL) and lysed by sonication at 4 °C. The proteins were bound to Nickel sepharose columns (GE Healthcare). The columns were washed with lysis buffer containing 30 mM imidazole. The proteins were eluted using a step gradient of imidazole in lysis buffer (50×, 100×, 150×, 2× 250 mM imidazole). All fractions were collected and monitored by SDS-polyacrylamide gel electrophoresis. After the addition of 5 mM DTT, the eluted proteins were treated overnight at 4 °C with TEV protease. The proteins were further purified by size exclusion chromatography on Superdex S200 16/60 HiLoad gel filtration columns (GE Healthcare) in 25 mM HEPES pH 7.5, 500 mM NaCl, 0.5 mM TCEP. Samples were monitored by SDS-polyacrylamide gel electrophoresis and the fractions containing DYRK1A or DYRK2 concentrated to 11 or 8 mg/mL, respectively. These protein samples were used for crystallization.

*Crystallization.* Leucettine L41 was added to the concentrated DYRK1A or DYRK2 proteins to a concentration of 1 mM. Crystals were grown using the vapor diffusion method, using 150 nL drops over a 20 $\mu$L reservoir. DYRK1A/leucettine L41 crystals grew at 4 °C from a 2:1 mixture of protein/reservoir solution over a reservoir consisting of 0.03 M $MgCl_2$, 22% poly(acrylic acid) 5100, 0.1 M HEPES, pH 8.2. DYRK2A/leucettine L41 crystals grew from a 2:1 ratio of protein/reservoir solution over a reservoir consisting of 0.20 M Na/KPO4, 20% PEG 3350, and 10% ethylene glycol.

PIM1 (6 mg/mL) was concentrated in the presence of leucettine L41 (1 mM final concentration) and a consensus peptide (ARKRRRHPSGPPTA-amide, 1 mM final concentration). Crystals were grown at 4 °C in 0.5 $\mu$L sitting drops mixing 0.4 $\mu$L of the solution with 0.1 $\mu$L of a reservoir solution containing 0.16 M sodium/potassium tartrate, 0.08 M Bis-Tris-propane pH 7.5, 16% PEG 3350, and 8% ethylene glycol.

Samples of the GSK-3$\beta$−axin (383−401) complex [6 mg/mL GSK-3$\beta$ + 0.37 mg/mL axin (383−401)] were incubated on ice with 400 $\mu$M leucettine L4 for 1 h prior to crystallization. Crystals of the GSK-3$\beta$−axin (383−401)/leucettine L4 complex were obtained within 3 days by hanging drop vapor diffusion method mixing 1 $\mu$L of complex with 1 $\mu$L of reservoir solution containing 0.1 M Tris-HCl pH 8.0, 0.15 M $MgCl_2$, and 15% (w/v) PEG 4000 at 20 °C.

Crystals belong to the hexagonal space group $P6_122$ and one copy of GSK-3$\beta$−axin (383−401)/leucettine L4 complex per crystallographic asymmetric unit.

*Data Collection and Structure Solution.* DYRK1A and DYRK2 crystals were cryoprotected using the well solution supplemented to 25% ethylene glycol and were flash frozen in liquid nitrogen. PIM1 crystals were similarly prepared but with 20% ethylene glycol. DYRK1A and DYRK2 data were collected at the Diamond Synchrotron, and PIM1 data was collected on an FR-E Superbright rotating Cu anode using an RAXIS image plate detector. Integration and scaling was carried out using MOSFLM[51] and SCALA.[52] Initial phases were calculated by molecular replacement with PHASER[53]

using structures of these same proteins available from the Protein Data Bank. Model building was done with COOT[54] and refinement was carried out in REFMAC5.[55] Data collection and refinement statistics can be found in Supporting Information Table S7.

GSK-3$\beta$–axin crystals were cryoprotected by the addition of 15% (v/v) glycerol and flash-cooled in a nitrogen stream at 100 K. Diffraction data to 2.77 Å resolution were collected on a Mar345 image plate mounted on a Rigaku RUH3R rotating-anode generator with Osmic optics operating at 100 mA and 50 kV. Integration was performed using the program XDS.[56] The structure was solved by molecular replacement with the program PHASER[53] employing the (pTyr216)–GSK-3$\beta$–axin (383–401) complex[50] (PDB code 1O9U) as search model. Bound ligand in the active site was identified by difference Fourier method. Structure refinement and model building was performed using iterative cycles of phenix.refine[57] and COOT.[54] Data collection and refinement statistics can be found in Supporting Information Table S8. The coordinates were deposited in the RCSB Protein Data Bank[58] with accession number 4B7T.

**Protein Kinase Assays.** *Protein Kinase Assay Buffers.* Buffer A: 10 mM $MgCl_2$, 1 mM EGTA, 1 mM DTT, 25 mM Tris-HCl pH 7.5, 50 $\mu$g heparin/mL

Buffer B: 50 mM $MgCl_2$, 90 mM NaCl, 30 mM Tris-HCl pH 7.4

*Kinase Preparations and Assays.* Kinase activities for each enzyme were assayed in buffer A or B, with their corresponding substrates, in the presence of 15 $\mu$M ATP in a final volume of 30 $\mu$L. After 30 min incubation at 30 °C, the reaction was stopped by harvesting, using a FilterMate harvester (Packard), onto P81 phosphocellulose papers (GE Healthcare), which were washed in 1% phosphoric acid. Scintillation fluid was added and the radioactivity measured in a Packard counter. Blank values were subtracted and activities calculated as pmoles of phosphate incorporated during the 30 min incubation. The activities were expressed in % of the maximal activity, i.e. in the absence of inhibitors. Controls were performed with appropriate dilutions of DMSO.

*CDK1/cyclin B* (M phase starfish oocytes, native), *CDK2/cyclin E* (human, recombinant, from A. Echalier), *CDK5/p25* (human, recombinant, expressed in *E. coli*), and *PIM1* (human, recombinant, expressed in *E. coli*) were assayed in buffer A (supplemented extemporaneously with 0.15 mg BSA/mL, except for CDK2) with 25 $\mu$g of histone H1.

*CDK7/cyclin H* (human, recombinant, expressed in insect cells) and *CDK9/cyclinT* (human, recombinant, expressed in insect cells) were assayed as described for CDK1/cyclin B but using 8.07 $\mu$g of CDK7/9-Tide (YSPTSPSYSPTSPSYSPTSPSKKKK).

*DYRK1A* (rat, recombinant, expressed in *E. coli* as GST fusion protein, provided by Dr. W. Becker), *DYRK1A, 1B, 2, 3* (human, recombinant, expressed in *E. coli* as GST fusion proteins), *DYRK4* (human, recombinant, expressed in insect cells), *CLK1, 2, 3,* and *4* (mouse, recombinant, expressed in *E. coli* as GST fusion proteins) were assayed as described for CDK1/cyclin B with 1 $\mu$g of RS peptide (GRSRSRSRSRSR) as a substrate. Native DYRK1A was purified from rat brain, taking advantage of the natural polyhistidine sequence located in the C-terminal domain of DYRK1A, by affinity chromatography on cobalt–sepharose beads (Clontech). Briefly, after a 30 min preclearing incubation at 4 °C with sepharose beads, rat brain lysates were incubated with cobalt–sepharose beads (400 $\mu$g total proteins/20 $\mu$L beads). Kinase activity of native DYRK1A was directly assessed on the beads in buffer A (+0.5 mg BSA/mL) using the Woodtide substrate (KKISGRLSPIMTEQ).

*GSK-3$\alpha$/$\beta$* (porcine brain, native, affinity purified on axin-sepharose beads), *GSK-3$\alpha$ and GSK-3$\beta$* (human, recombinant, expressed in insect cells) and *PfGSK-3* (*Plasmodium falciparum*, recombinant, expressed in *E. coli*) were assayed as described for CDK1/cyclin B but using a GSK-3 specific substrate (GS-1: YRRAAVPPSPSLSRHSSPHQpSEDEEE where pS stands for phosphorylated serine).

*Casein kinase 1 (CK1$\delta$/$\varepsilon$)* (porcine brain, native) and *LmCK1* (*Leishmania major*, recombinant, expressed in *E. coli*) were assayed with 0.67 $\mu$g of CKS peptide (RRKHAAIGpSAYSITA), a CK1 specific substrate.

*Casein kinase 2 (CK2)* (human, recombinant, obtained from C. Cochet) was assayed in buffer B, with 7.79 $\mu$g of peptide substrate 29 (RRREDEESDDEE).

*Erk2* (rat, recombinant) was assayed as described for CDK1/cyclin B with 2.35 $\mu$g of the specific substrate Ets1 (amino acids 1–138) in buffer A.

*Native Kinase Preparations and Assays.* Native, endogenous kinase activities from cell cultures were assayed following either immunoprecipitation (DYRK1A, see below) or affinity chromatography purification (GSK-3, see below). Kinases were assayed in buffer C, at 30 °C, at a final ATP concentration of 15 $\mu$M. Blank values were subtracted and activities expressed in percent of the maximal activity, i.e. in the absence of inhibitors. Controls were performed with appropriate dilutions of DMSO. DYRK1A was purified by immunoprecipitation of 1.3 mg HT22 cell extract protein diluted in phosphate buffered saline (PBS, Gibco) supplemented with protease inhibitor cocktail (Complete, Roche) on Pierce Protein G Agarose (Thermo Scientific) using 2 $\mu$g DYRK1A antibody (Abnova). After immunoprecipitation, Protein G agarose beads were washed with Bead buffer then buffer C (see Affinity Chromatography Buffers below). The kinase activity was assayed in buffer C using Woodtide (1 $\mu$g/assay) as a substrate, in the presence of 15 $\mu$M [$\gamma$-33P] ATP (3000 Ci/mmol; 10 mCi/mL) in a final volume of 30 $\mu$L. After 30 min incubation at 30 °C, the reaction was stopped by harvesting onto P81 phosphocellulose paper filters (Whatman). The filters were washed in 1% phosphoric acid and were counted in the presence of ACS (Amersham) scintillation fluid.

Endogenous GSK-3 was purified from HT22 cell extract (0.5 mg protein) by affinity chromatography on axin-agarose beads (GSK-3).[25] After extensive washing the bound kinase activity was assayed as described above.

**Kinase Interaction Panel (Ambit Biosciences/DiscoveRx).** Assays were performed essentially as described previously.[18] For most assays, kinase-tagged T7 phage strains were grown in parallel in 24-well blocks in an *E. coli* host derived from the BL21 strain. *E. coli* were grown to log-phase and infected with T7 phage from a frozen stock (multiplicity of infection ~0.1) and incubated with shaking at 32 °C until lysis (~90 min). The lysates were centrifuged (6000*g*) and filtered (0.2 $\mu$m) to remove cell debris. The remaining kinases were produced in HEK-293 cells and subsequently tagged with DNA for qPCR detection. Streptavidin-coated magnetic beads were treated with biotinylated small molecule ligands for 30 min at room temperature (RT) to generate affinity resins for kinase assays. The liganded beads were blocked with excess biotin and washed with blocking buffer (SeaBlock (Pierce), 1% BSA, 0.05% Tween 20, 1 mM DTT) to remove unbound ligand and to reduce nonspecific phage binding. Binding reactions were assembled by combining kinases, liganded affinity beads, and test compounds in 1× binding buffer (20% SeaBlock, 0.17× PBS, 0.05% Tween 20, 6 mM DTT). An 11-point 3-fold serial dilution of each test compound was prepared in 100% DMSO at 100× final test concentration which subsequently diluted to 1× in the assay. All reactions were performed in polystyrene 96-well plates in a final volume of 0.135 mL. The assay plates were incubated at RT with shaking for 1 h, and the affinity beads were washed four times with wash buffer (1× PBS, 0.05% Tween 20). The beads were then resuspended in elution buffer (1× PBS, 0.05% Tween 20, 0.5 $\mu$M nonbiotinylated affinity ligand) and incubated at RT with shaking for 30 min. The kinase concentration in the eluates was measured by qPCR. $K_d$s were determined using 11-point dose–response curves (top concentration 30 $\mu$M, 3-fold dilutions down) which were performed in duplicate. The $K_d$ reported represents the average of the duplicates and a value of 40000 nM indicates that no binding was seen at the highest concentration tested (>30 $\mu$M).

**Affinity Chromatography: Leucettine L41 Targets in Mouse Brain.** *In Vitro Association Experiments.* First, 2.5 g mouse brain tissue, frozen in liquid nitrogen, was pestled in a mortar to fine powder and resuspended in 15 mL of lysis buffer containing 20 mM HEPES, pH 7.5, 150 mM NaCl, 0.25% Triton X-100, 1 mM EDTA, 1 mM EGTA, and 1 mM DTT plus additives (10 $\mu$g/mL aprotinin, 10 $\mu$g/mL leupeptin, 1 mM PMSF, 1 mM $Na_3VO_4$, 10 mM NaF). Then the

suspension was homogenized on ice for 3 × 30 s using a Ultra-Turrax T8 disperser equipped with a S10N-5G dispersing element (IKA). In vitro association experiments were performed essentially as described,[59] with the exception that KinAffinity beads (Kinaxo Biotechnologies), representing a set of different broad-spectrum kinase inhibitors immobilized on Sepharose beads, were applied for affinity chromatography and for competition experiments and tissue extracts were treated with different concentrations of leucettine L41 (0 nM, 1 nM, 10 nM, 100 nM, 1 μM, 10 μM, 100 μM) for 30 min prior to addition of inhibitor beads and incubation for an additional 2.5 h at 4 °C. Alternatively, free inhibitor and KinAffinity beads were added simultaneously to the tissue extract.

*Mass Spectrometry Sample Preparation.* Proteins enriched with the KinAffinity beads were digested on the beads using an in-solution procedure. Briefly, per condition, 100 μL of digestion buffer (8 M urea, 50 mM Tris pH 8.2, 10 mM sodium pyrophosphate, 5 mM EDTA, 5 mM EGTA, 10 mM sodium fluoride, 10 mM β-glycerophosphate, 10 mM sodium orthovanadate, phosphatase inhibitor cocktail 2 and 3 (Sigma, 1:100 (v/v)) and Complete Protease Inhibitor Cocktail Tablets (Roche) were added. Samples were then reduced with 1 mM DTT for 30 min at RT and then alkylated with 5.5 mM chloroacetamide for 45 min at RT. Proteins were initially cleaved with lysyl endopeptidase (Wako, 0.3 μg per sample) for 4 h and diluted five times with 20 mM Tris·HCl pH 8.2 prior to overnight proteolytic cleavage with trypsin (Promega, 0.5 μg per sample). The peptide mixtures were acidified by the addition of TFA to a final concentration of 0.4% and subsequently desalted via $C_{18}$ Sep-Pak columns (Waters). Peptides were eluted with 50% acetonitrile, 0.5% acetic acid, frozen in liquid nitrogen, and lyophilized. To enable subsequent quantitative MS analysis, peptides were labeled by means of stable isotope dimethyl labeling as described.[60] Briefly, dried peptides of one sample were reconstituted in 100 μL of 100 mM TEAB (pH 5−8.5) and substituted with the respective formaldehyde and sodium cyanoborohydride solutions for the labeling reactions to result in light (Δ28 $m/z$), medium (Δ32 $m/z$), or heavy (Δ36 $m/z$) peptide entities. After quenching the labeling reactions, the light, medium, and heavy peptide entities belonging to one KinAffinity experiment were combined, frozen in liquid nitrogen, and lyophilized. To reduce sample complexity, each sample was separated into three fractions prior to LC-MS analysis. Therefore, samples were reconstituted in 100 μL of SCX buffer A (7 mM $KH_2PO_4$, 30% acetonitrile, pH 2.65) and loaded onto in-house made cation-StageTips (3M, Empore Cation-SR). Fraction 1 represents the flow through combined with an elution at 15% SCX buffer B (SCX buffer A containing 350 mM KCl), and fractions 2 and 3 contain peptides eluted with 45% and 100% SCX buffer B, respectively. Peptides of each fraction were then desalted and enriched using in-house made $C_{18}$ STAGE Tip columns.[61] Eluted peptides were concentrated to a final volume of 2 μL in a vacuum concentrator 5301 (Eppendorf) and substituted with 10 μL of 0.5% acetic acid before MS analysis.

*Mass Spectrometry Analysis.* LC-MS/MS analysis was performed on an LTQ-Orbitrap Velos mass spectrometer (Thermo Fisher Scientific). The sample was loaded by an Easy n-LC II nanoflow system (Thermo Fischer Scientific) on a 15 cm fused silica emitter (New Objective) packed in-house with reversed phase material (Reprusil-Pur C18-AQ, 3 μm, Dr. Maisch GmbH) at a flow of 500 nL/min. The bound peptides were eluted by 140 min runs comprised of a segmented gradient from 10% to 30% of solvent B (80% acetonitrile, 0.5% acetic acid) over 96 min, 30−50% of solvent B over 12 min, and 50−60% of solvent B over 7 min at a flow rate of 200 nL/min. Peptides were sprayed directly into the mass spectrometer using a nanoelectrospray ion source (ProxeonBiosystems). The mass spectrometer was operated in the positive ion mode with application of a data dependent mode to automatically switch between MS and MS/MS acquisition and a dynamic exclusion for the subsequent 90 s of ions once selected for fragmentation. To improve mass accuracy in the MS mode, the lock-mass option was enabled as described.[62] Full scans were acquired in the orbitrap at a resolution $R$ = 60000 and a target value of 1000000 ions. The 15 most intense ions detected in the MS scan were selected for collision induced dissociation in the LTQ at a target value of 5000 ion counts. General used mass spectrometric settings were: spray voltage, 2.2 kV; no sheath and auxiliary gas flow; heated capillary temperature, 220 °C; normalized collision energy, 35%, and an activation $q$ = 0.25.

*Data Processing.* MS raw files were collectively processed with the MaxQuant software suite version 1.2.0.32.[63] Peak lists were searched against the mouse swissprot database version 2011_07 using the Andromeda search engine.[64] Trypsin was selected as the proteolytic enzyme, and we required a minimal peptide length of six amino acids and maximal two missed cleavage sites were allowed. Carbamidomethylation of cysteine residues was set as fixed modification while oxidation of methionine and protein *N*-acetylation were allowed as variable modifications. For peptide quantification the "match between runs" function was enabled with a 2 min time window.

**Affinity Chromatography on Immobilized Leucettine L41.** *Affinity Chromatography Buffers.* Bead buffer: 50 mM Tris (pH 7.4), 5 mM NaF, 250 mM NaCl, 5 mM EDTA, 5 mM EGTA, 0.1% Nonidet P-40 and protease inhibitor cocktail

Blocking buffer: 1 M ethanolamine in coupling buffer, pH 8.0

Coupling buffer: 0.1 M $NaHCO_3$ and 0.2 M NaCl, pH 8.3

Homogenization buffer: 60 mM β-glycerophosphate, 15 mM *p*-nitrophenylphosphate, 25 mM Mops (pH 7.2), 15 mM EGTA, 15 mM $MgCl_2$, 2 mM dithiothreitol, 1 mM sodium orthovanadate, 1 mM sodium fluoride, 1 mM phenylphosphate disodium, and protease inhibitor cocktail

Washing buffer: 0.1 M $CH_3COONa$, pH 4

Buffer C: 60 mM β-glycerophosphate, 30 mM *p*-nitrophenylphosphate, 25 mM Mops (pH 7.2), 5 mM EGTA, 15 mM $MgCl_2$, 1 mM DTT, 0.1 mM sodium vanadate, 1 mM phenylphosphate.

*Preparation of Leucettine L41 Agarose Beads.* CNBr-activated sepharose 4B (Sigma) was swollen in cold 1 mM HCl for 30 min. Beads were then activated with coupling buffer. Leucettine L41 (12 μmol L41/mL beads) was coupled overnight under constant rotation at RT. After removal of the supernatant, residual active sites were quenched using blocking buffer for 2 h 30 min under constant rotation at RT. Beads were washed with coupling buffer, washing buffer, and bead buffer and brought to a 20% suspension in bead buffer. They were stored at 4 °C until further use. Ethanolamine beads were used as controls.

*Preparation of Brain and HT22 Cell Extracts.* Mice brains were obtained from the animal facility of the University of Rennes and snap-frozen until further use. Tissues were weighed, homogenized, and sonicated in homogenization buffer (5 mL/g of material). Homogenates were centrifuged for 15 min at 17000*g* at 4 °C. The supernatant was recovered, assayed for protein content (BioRad Protein Assay), and directly added on the beads.

HT22 murine hippocampal neuronal cells (see below) were subcultured once every 2 days. When cells reached 80% confluence, they were washed with PBS, pelleted at 1000*g* for 3 min at 4 °C, homogenized, and sonicated in homogenization buffer (250 μL/pellet).

*Affinity Chromatography of Leucettine L41-Interacting Proteins.* Just before use, 20 μL of packed leucettine L41 beads were washed with 1 mL of bead buffer and resuspended in this buffer. After a brief spin at 17000*g*, the brain tissue or HT22 cells extract supernatants (1 mg total protein) was loaded on 20 μL of packed beads and the volume was adjusted to 1 mL with bead buffer in the presence or absence of 100 μM leucettine L41. The tubes were rotated at 4 °C for 30 min. After a brief spin at 10000*g* and removal of the supernatant, the beads were washed four times with bead buffer before addition of 80 μL of 2× LDS sample buffer (Invitrogen) or Laemmli sample buffer (Bio-Rad) and 200 mM DTT. Following heat denaturation for 3 min, the bound proteins were analyzed by SDS-PAGE and Western blotting as described below.

**Cell Culture and Cell Survival Assessment.** HT22 murine hippocampal neuronal cells (a gift from Dr. David Schubert, Salk Institute, La Jolla, CA) were maintained in Dulbecco's Modified Eagle's Medium (DMEM, with L-glutamine, Gibco), supplemented with 10% (v/v) fetal bovine serum (Gibco), 1% penicillin/streptomycin (Fisher Scientific, Pen Strep solution), and incubated

at 37 °C under 5% $CO_2$ . Cells were subcultured once every 2 days. Leucettine L41 treatments at the indicated concentrations were performed on 80% confluent cultures for 4 h. Control experiments were carried out using appropriate dilutions of DMSO.

MG132 treatments were performed on HT22 cells in the presence or absence of different concentrations of leucettine L41, 10 $\mu$M 6BIO, or 10 $\mu$M alsterpaullone. Control experiments were carried out using 0.5% DMSO. Cells were seeded at 0.25 million cells per well in 6-well culture plates for 24 h before treatments.

Glutamate treatments at the indicated times and concentrations were performed on HT22 cells in the presence or absence of leucettine L41. Cells were seeded at 4000 cells per well in 96-well culture plates for 24 h before treatments. Control experiments were carried out using appropriate dilutions of leucettine L41 (maximum 1% DMSO). Cell viability was determined by measuring the reduction of MTS as described previously.[65]

*Electrophoresis and Western Blotting.* Cells were resuspended, lysed in homogenization buffer, and sonicated. After centrifugation (17000*g* for 15 min at 4 °C), the protein concentration was determined in the supernatants with the Bradford protein assay (Bio-Rad, Marnes-la-Coquette, France). Following heat denaturation, proteins were separated by 10% NuPAGE precast Bis-Tris (10% Bis-Tris gel 1 mm) mini gel electrophoresis system (Invitrogen) with MOPS SDS. Proteins were transferred to 0.45 $\mu$m nitrocellulose filters (Schleicher and Schuell). These were blocked with 5% low-fat milk in Tris-buffered saline−Tween-20, incubated overnight at 4 °C with specific antibodies, and analyzed by enhanced chemiluminescence (ECL, Amersham). Antibodies were directed against DYRK1A (Abnova; dilution 1:1000), CK2$\alpha/\alpha'$ (C. Cochet, 1:1000), CK2$\beta$ (C. Cochet, 1:500), GSK-3$\beta$ (Stressgen, 1:1000), Vac14 (Sigma, 1:750), Fig4 (NeuroMab N202/7, 1/200), PIKfyve (Calbiochem, 1:2000), $\beta$-catenin (Millipore, 1:1000), phospho-$\beta$-catenin (Cell Signaling, 1:500).

**CLK1 Alternative Splicing in HT22 Cells.** Total mRNA was isolated from cultured HT22 hippocampal cells either treated for 6 h with leucettine L41, in a dose-dependent manner, or with DMSO (1%), using an RNeasy Plus Mini extraction kit (Qiagen) following the manufacturer's instructions. The concentration and quality of the RNA were determined by spectrophotometry and agarose gel electrophoresis. Finally, 1 $\mu$g of total RNA was reverse-transcribed using the Superscript III ReverseTranscript kit (Invitrogen) according to the manufacturer's instructions.

PCR reactions were performed using Taq DNA polymerase (Roche) (for actin and CLK1) or Pwo DNA polymerase (Roche) (for CLK4), 400 nM of each primer, and 50 ng of cDNA template for each reaction. CLK1 primers were based on those mentioned in ref 66, while CLK4 and actin primers were designed using Web-based Primer 3 software (http://frodo.wi.mit.edu/primer3/). All primers were synthesized by Eurogentec.

The oligonucleotide sequences were as follows:

Actin forward: 5′-CAC-CCG-CGA-GCA-CAG-CTT-CT-3′
Actin reverse: 5′-TTG-CAC-ATG-CCG-GAG-CCG-TT-3′
CLK-1 forward: 5′-ATG-GAG-AAC-CTG-GAA-GCA-GA-3′
CLK-1 reverse: 5′-CCG-AAA-GCA-CCT-TCA-CCT-AA-3′
CLK-4 forward: 5′-GCC-CTA-AGA-GAA-AGC-GTA-A-3′
CLK-4 reverse: 5′-TCA-CCT-AAA-GTG-TCC-ACG-A-3′

For actin ($T_m$: 64 °C) and CLK1 ($T_m$: 60 °C), PCR conditions were 94 °C for 3 min, 35 cycles of amplification (94 °C for 30 s, $T_m$ °C for 30 s, 72 °C for 30 s), and 72 °C for 7 min. For CLK4 ($T_m$: 56 °C), PCR conditions were 94 °C for 3 min, 30 cycles of amplification (94 °C for 20 s, $T_m$ °C for 30 s, 72 °C for 1 min), and 72 °C for 7 min.

**Brain Slice Preparation, Biolistic Transfection, and Compound Evaluation.** Brain slices were prepared from postnatal day 10 (P10) CD Sprague−Dawley rats (Charles River, Wilmington, MA). Rat pups were sacrificed in accordance with NIH guidelines and under Duke IACUC approval and oversight. then 250 $\mu$m thick coronal sections from the middle third of the brain were cut using a vibratome (Vibratome Company, St Louis, MO) and placed in long-term tissue culture medium as previously described[67] and incubated under 5% $CO_2$ in humidified chambers. A custom-modified biolistic device (Helios Gene Gun, BioRad, Hercules, CA) was used for particle-mediated transfection immediately after slicing. Elemental gold particles were used, upon which the desired DNA plasmids were precipitated as per manufacturer's instructions and previously published detailed protocols.[67] Compounds were dissolved in DMSO and supplemented to the culture medium at concentrations indicated at a final concentration of 0.1% DMSO. Brain slice explants were incubated for 3 days before neurodegeneration outcome measures were made.

For siRNA experiments, siRNAdel gold carrier particles (Seashell Technology, La Jolla, CA) were first coated with a mixture (66 pmol each/1.5 mg gold nanoparticles) of three siRNAs targeting DYRK1A (Eurogentec), or a "Universal Negative Control" control siRNA (Integrated DNA Technologies (IDT)), per manufacture's instruction, followed by coating with DNA plasmids and biolistic delivery as described above. The A2, R2 and R3 siRNAs were, respectively: CUCGGAUUCAACCUUAUUA, GGAUGUAUCUUGGUUGAAA, and AUGGAGCUAUGGACGUUAA.

*Expression Constructs.* The APP expression constructs were made by subcloning human neural APP sequence (695 aa form) into the Gwiz expression vector (Genlantis, San Diego, CA). The EYFP visual reporter was also subcloned into the Gwiz vector, which we have previously shown to yield sustained expression for >1 week in numerous brain regions and cell types including cortical pyramidal neurons.[31b,d]

*Neuronal Health and Statistics.* For the assessment of numbers of healthy cortical pyramidal neurons, brain slices were imaged on a Leica MZIIIFL fluorescence stereomicroscope. Pyramidal neurons were identified based on their characteristic positioning and orientation within the cortical plate and by their extension of a single, prominent apical dendrite radially toward the pial surface. The key criteria used to determine numbers of healthy cortical pyramidal neurons were (1) a robust and brightly labeled cell body positioned within the pyramidal neuronal layers of the cortex, (2) a single and clear apical primary dendrite, (3) two or more clear basilar primary dendrites greater than 2 cell body diameters long, and (4) clear and continuous cytoplasmic labeling with EYFP through the cell body and dendritic and axonal compartments. ANOVA followed by Dunnett's post hoc comparison test at the 0.05 confidence level was used for assessing statistical significance with $N = 12$ brain slices per condition. Each experiment was carried out at least three times.

## ■ ASSOCIATED CONTENT

### Ⓢ Supporting Information

Tables, figures, and chemistry experimental procedures. This material is available free of charge via the Internet at http://pubs.acs.org.

### Accession Codes

The models and structure factors of DYRK1A, DYRK2, and PIM1 in complex with leucettine L41 are deposited with PDB accession codes 4AZE, 4AZF, and 4GW8, respectively. GSK-3/leucettine L4 accession code is 4B7T.

## ■ AUTHOR INFORMATION

### Corresponding Author

*Phone: +33. (0)2.98.72.94.92. E-mail: meijer@manros-therapeutics.com.

### Notes

The authors declare the following competing financial interest(s): L.M., J.P.B., and F.C. are co-inventors of a patent on leucettines. L.M. is president and CSO of ManRos Therapeutics, which has an exclusive license on the leucettine patent.

## ■ ACKNOWLEDGMENTS

We are grateful to our colleagues for laboratory reagents and photographs: W. Becker, C. Debitus, A. Echalier, Y. Ferandin, H. Galons, N. Gray, B. Joseph, C. Kunick, F. Lesourd, M. Menke, G. Mettey, G.R. Pettit, D. Schubert, and L. Skaltsounis. We thank C. Benesteau and L. Bernard-Touami (University of Rennes, BIOSIT Animal Facility) for providing mouse tissue samples. This research was supported by grants from the "Fonds Unique Interministériel" (FUI) PHARMASEA project (L.M., J.P.B., F.C.), the "Association France-Alzheimer (Finistère)" (L.M.), "CRITT-Santé Bretagne" (L.M.), and "Fondation Jérôme Lejeune" (L.M.), the "Anna's Angels Down Syndrome Research Foundation" (R.S.S., D.C.L.), and the "Caroline Ball Family Fund" (R.S.S., D.C.L.). The SGC is a registered charity (no. 1097737) that receives funds from the Canadian Institutes for Health Research, the Canada Foundation for Innovation, Genome Canada, GlaxoSmithKline, Pfizer, Eli Lilly, the Novartis Research Foundation, Takeda, the Ontario Ministry of Research and Innovation, and the Wellcome Trust.

## ■ ABBREVIATIONS USED

AD, Alzheimer's disease; APP, amyloid precursor protein; BSA, bovine serum albumin; 6BIO, 6-bromo-indirubin-3′-oxime; CDKs, cyclin-dependent kinases; CK1, casein kinase 1; CK2, casein kinase 2; CLKs, cdc2-like kinases; DYRKs, dual specificity, tyrosine phosphorylation regulated kinases; DMEM, Dulbecco's Modified Eagle's Medium; DMSO, dimethylsulfoxide; DTT, dithiothreitol; EYFP, enhanced yellow fluorescent protein; FBS, fetal bovine serum; GSH, glutathione; GSK-3, glycogen synthase kinase-3; GST, glutathione-*S*-transferase; IPTG, isopropyl-*β*-D-thiogalactopyranoside; LB-broth, Luria–Bertani medium; MTS, 3-(4,5-dimethylthiazol-2-yl)-5-(3-carboxymethoxyphenyl)-2-(4-sulfophenyl)-2*H*-tetrazolium; NMDA, *N*-methyl-D-aspartate; PBS, phosphate-buffered saline; PIKfyve, phosphatidylinositol-3-phosphate 5-kinase type III; PIP3P, phosphatidylinositol-3-phosphate; PI(3,5)$P_2$, phosphatidylinositol-3,5-bisphosphate; RT, room temperature; SAR, structure–activity relationship; SLK, STE20-like Ser/Thr protein kinase

## ■ REFERENCES

(1) (a) Kostich, M.; English, J.; Madison, V.; Gheyas, F.; Wang, L.; Qiu, P.; Greene, J.; Laz, T. M. Human members of the eukaryotic protein kinase family. *Genome Biol.* **2002**, *3*(9), doi 10.1186/gb-2002-3-9-research0043. (b) Manning, G.; Whyte, D. B.; Martinez, R.; Hunter, T.; Sudarsanam, S. The protein kinase complement of the human genome. *Science* **2002**, *298*, 1912–1934.

(2) (a) Weinmann, H.; Metternich, R. Drug discovery process for kinase inhibitors. *ChemBioChem* **2005**, *6*, 455–459. (b) Norman, P. Kinase therapeutics pipelines: an assessment of targets and agents in development. *Insight Pharma Report*, 2007; 175 pp. (c) Eglen, R. M.; Reisine, T. The current status of drug discovery against the human kinome. *Assay Drug Dev. Technol.* **2009**, *7*, 22–43. (d) Eglen, R.; Reisine, T. Drug discovery and the human kinome: recent trends. *Pharmacol. Ther.* **2011**, *130*, 144–156. (e) Via, M. C. *Kinase-Targeted Therapeutics: Development Pipelines, Challenges, and Opportunities*; Cambridge Healthtech Institute: Needham, MA, 2011; 124 pp.

(3) Fedorov, O.; Müller, S.; Knapp, S. The (un)targeted cancer kinome. *Nature Chem. Biol.* **2010**, *6*, 166–169.

(4) (a) Aranda, S.; Laguna, A.; de la Luna, S. DYRK family of protein kinases: evolutionary relationships, biochemical properties, and functional roles. *FASEB J.* **2011**, *25*, 449–462. (b) Becker, W.; Sippl, W. Activation, regulation, and inhibition of DYRK1A. *FEBS J.* **2011**, *278*, 246–256. (c) Tejedor, F. J.; Hämmerle, B. MNB/DYRK1A as a multiple regulator of neuronal development. *FEBS J.* **2011**, *278*, 223–235. (d) Wegiel, J.; Gong, C. X.; Hwang, Y. W. The role of DYRK1A in neurodegenerative diseases. *FEBS J.* **2011**, *278*, 236–245.

(5) (a) Yun, B.; Farkas, R.; Lee, K.; Rabinow, L. The Doa locus encodes a member of a new protein kinase family and is essential for eye and embryonic development in *Drosophila melanogaster*. *Genes Dev.* **1994**, *8*, 1160–1173. (b) Nayler, O.; Stamm, S.; Ullrich, A. Characterization and comparison of four serine- and arginine-rich (SR) protein kinases. *Biochem. J.* **1997**, *326*, 693–700. (c) Hagiwara, M. Alternative splicing: a new drug target of the post-genome era. *Biochim. Biophys. Acta* **2005**, *1754*, 324–331.

(6) Debdab, M.; Renault, S.; Soundararajan, M.; Fedorov, O.; Filippakopoulos, P.; Lozach, O.; Babault, L.; Tahtouh, T.; Baratte, B.; Ogawa, Y.; Hagiwara, M.; Eisenreich, A.; Rauch, U.; Knapp, S.; Meijer, L.; Bazureau, J.-P. Leucettines, a class of potent inhibitors of cdc2-like kinases and dual specificity, tyrosine phosphorylation regulated kinases derived from the marine sponge leucettamine B: modulation of alternative pre-RNA splicing. *J. Med. Chem.* **2011**, *54*, 4172–4186.

(7) (a) Chan, G. W.; Mong, S.; Hemling, M. E.; Freyer, A. J.; Offen, P. M.; De Brosse, C. W.; Sarau, H. M.; Westley, J. W. New leukotriene B4 receptor antagonist: leucettamine A and related imidazole alkaloids from the marine sponge *Leucetta microraphis*. *J. Nat. Prod.* **1993**, *56*, 116–121. (b) Watanabe, K.; Tsuda, Y.; Iwashima, M.; Iguchi, K. A new bioactive triene aldehyde from the marine sponge *Leucetta microraphis*. *J. Nat. Prod.* **2000**, *63*, 258–260.

(8) (a) Davis, R. A.; Aalbersberg, W.; Meo, S.; Moreira da Rocha, R.; Ireland, C. M. The isolation and synthesis of polyandrocarpamines A and B. Two new 2-aminoimidazolone compounds from the Fijian ascidian *Polyandrocarpa* sp. *Tetrahedron Lett.* **2002**, *58*, 3263–3269. (b) Davis, R. A.; Baron, P. S.; Neve, J. E.; Cullinane, C. A microwave-assisted stereoselective synthesis of polyandrocarpamines A and B. *Tetrahedron Lett.* **2008**, *50*, 880–882.

(9) (a) Lindel, T.; Hoffmann, H. Synthesis of dispacamide from the marine sponge *Agelas dispar*. *Tetrahedron Lett.* **1997**, *38*, 8935–8938. (b) Fresneda, P. M.; Molina, P.; Sanz, M. A. A convergent approach to midpacamide and dispacamide pyrrole-imidazole marine alkaloids. *Tetrahedron Lett.* **2001**, *42*, 851–854. (c) Travert, N.; Al-Mourabit, A. A likely biogenetic gateway linking 2-aminoimidazolinone metabolites of sponges to proline: spontaneous oxidative conversion of the pyrrole–proline–guanidine pseudo-peptide to dispacamide A. *J. Am. Chem. Soc.* **2004**, *126*, 10252–10253. Erratum in: *J. Am. Chem. Soc.* **2005**, *127*, 10454.

(10) (a) Hollenbeak, K. H.; Schmitz, F. J. Aplysinopsin: antineoplastic tryptophan derivative from the marine sponge *Verongia spengelii*. *Lloydia* **1977**, *40*, 479–481. (b) Singh, S. N.; Bhatnagar, S.; Fatma, N.; Chauhan, P. M.; Chatterjee, R. K. Antifilarial activity of a synthetic marine alkaloid, aplysinopsin (CDRI Compound 92/138). *Trop. Med. Int. Health* **1997**, *2*, 535–543.

(11) Roué, M.; Domart-Coulon, I.; Ereskovsky, A.; Djediat, C.; Perez, T.; Bourguet-Kondracki, M. L. Cellular localization of clathridimine, an antimicrobial 2-aminoimidazole alkaloid produced by the Mediterranean calcareous sponge *Clathrina clathrus*. *J. Nat. Prod.* **2010**, *73*, 1277–1282.

(12) (a) Cimino, G.; de Rosa, S.; de Stefano, S.; Mazzarella, L.; Puliti, R.; Sodano, G. Isolation and X-ray crystal structure of a novel bromo-compound from two marine sponges. *Tetrahedron Lett.* **1982**, *23*, 767–768. (b) Sharma, G. M.; Buyer, J.; Pomerantz, M. W. Characterization of a yellow compound isolated from the marine sponge *Phakellia flabellata*. *J. Chem. Soc., Chem. Commun.* **1980**, *10*, 435–436. (c) Williams, D. H.; Faulkner, J. Isomers and tautomers of hymenialdisine and debromohymenialdisine. *Nat. Prod. Lett.* **1996**, *9*, 57–64. (d) Xu, Y. Y.; Yakushijin, K.; Horne, D. A. Synthesis of C(11)N(5) Marine sponge alkaloids: (±)-hymenin, stevensine, hymenialdisine, and debromohymenialdisine. *J. Org. Chem.* **1997**, *62*, 456–464. (e) Papeo, G.; Posteri, H.; Borghi, D.; Varasi, M. A new glycociamidine ring precursor: syntheses of (*Z*)-hymenialdisine, (*Z*)-2-debromohymenialdisine, and (±)-endo-2-debromohymenialdisine. *Org. Lett.* **2005**, *7*, 5641–5644. (f) Nguyen, T. N.; Tepe, J. J.

Preparation of hymenialdisine, analogues and their evaluation as kinase inhibitors. *Curr. Med. Chem.* **2009**, *16*, 3122−3143. (g) Meijer, L.; Thunnissen, A. M. W. H.; White, A.; Garnier, M.; Nikolic, M.; Tsai, L. H.; Walter, J.; Cleverley, K. E.; Salinas, P. C.; Wu, Y. Z.; Biernat, J.; Mandelkow, E. M.; Kim, S.-H.; Pettit, G. R. Inhibition of cyclin-dependent kinases, GSK-3$\beta$ and casein kinase 1 by hymenialdisine, a marine sponge constituent. *Chem. Biol.* **2000**, *7*, 51−63. (h) Wan, Y.; Hur, W.; Cho, C. Y.; Liu, Y.; Adrian, F. J.; Lozach, O.; Bach, S.; Mayer, T.; Fabbro, D.; Meijer, L.; Gray, N. S. Synthesis and target identification of hymenialdisine analogs. *Chem. Biol.* **2004**, *11*, 247−259.

(13) (a) Molina, P.; Almendros, P.; Fresneda, P. M. An iminophosphorane-mediated efficient synthesis of the alkaloid leucettamine B of marine origin. *Tetrahedron Let.* **1994**, *35*, 2235−2236. (b) Roué, N. Bergman, Synthesis of the marine alkaloid leucettamine B. *Tetrahedron* **1999**, *55*, 14729−14738.

(14) Debdab, M.; Renault, S.; Eid, S.; Lozach, O.; Meijer, L.; Carreaux, F.; Bazureau, J.-P. An efficient method for the preparation of new analogs of leucettamine B under solvent-free microwave irradiation. *Tetrahedron Let.* **2009**, *78*, 1191−1203.

(15) (a) Bain, J.; Plater, L.; Elliott, M.; Shpiro, N.; Hastie, C. J.; McLauchlan, H.; Klevernic, I.; Arthur, J. S.; Alessi, D.; Cohen, P. The selectivity of protein kinase inhibitors: a further update. *Biochem. J.* **2007**, *408*, 297−315. (b) Seifert, A.; Allan, L. A.; Clarke, P. R. DYRK1A phosphorylates caspase 9 at an inhibitory site and is potently inhibited in human cells by harmine. *FEBS J.* **2008**, *275*, 6268−6280. (c) Göckler, N.; Jofre, G.; Papadopoulos, C.; Soppa, U.; Tejedor, F. J.; Becker, W. Harmine specifically inhibits protein kinase DYRK1A and interferes with neurite formation. *FEBS J.* **2009**, *276*, 6324−6337. (d) Adayev, T.; Wegiel, J.; Hwang, Y. W. Harmine is an ATP-competitive inhibitor for dual-specificity tyrosine phosphorylation-regulated kinase 1A (Dyrk1A). *Arch. Biochem. Biophys.* **2011**, *507*, 212−218. (e) Frost, D.; Meechoovet, B.; Wang, T.; Gately, S.; Giorgetti, M.; Shcherbakova, I.; Dunckley, T. $\beta$-Carboline compounds, including harmine, inhibit DYRK1A and tau phosphorylation at multiple Alzheimer's disease-related sites. *PLoS One* **2011**, *6*, e19264.

(16) (a) Brierley, D. I.; Davidson, C. Developments in harmine pharmacology—implications for ayahuasca use and drug-dependence treatment. *Prog. Neuropsychopharmacol. Biol. Psychiatr.* **2012**, doi 10.1016/j.pnpbp.2012.06.001. (b) Grabher, P.; Durieu, E.; Kouloura, I.; Halabalaki, M.; Skaltsounis, L. A.; Meijer, L.; Hamburge, M.; Potterat, O. Library-based discovery of DYRK1A/CLK1 inhibitors from natural product extracts. *Planta Med.* **2012**, *78*, 951−956.

(17) Muraki, M.; Ohkawara, B.; Hosoya, T.; Onogi, H.; Koizumi, J.; Koizumi, T.; Sumi, K.; Yomoda, J.; Murray, M. V.; Kimura, H.; Furuichi, K.; Shibuya, H.; Krainer, A. R.; Suzuki, M.; Hagiwara, M. Manipulation of alternative splicing by a newly developed inhibitor of Clks. *J. Biol. Chem.* **2004**, *279*, 24246−24254.

(18) (a) Fabian, M. A.; Biggs, W. H.; Treiber, D. K.; Atteridge, C. E.; Azimioara, M. D.; Benedetti, M. G.; Carter, T. A.; Ciceri, P.; Edeen, P. T.; Floyd, M.; Ford, J. M.; Galvin, M.; Gerlach, J. L.; Grotzfeld, R. M.; Herrgard, S.; Insko, D. E.; Insko, M. A.; Lai, A. G.; Lélias, J. M.; Mehta, S. A.; Milanov, Z. V.; Velasco, A. M.; Wodicka, L. M.; Patel, H. K.; Zarrinkar, P. P.; Lockhart, D. J. A small molecule−kinase interaction map for clinical kinase inhibitors. *Nature Biotechnol.* **2005**, *23*, 329−336. (b) Karaman, M. W.; Herrgard, S.; Treiber, D. K.; Gallant, P.; Atteridge, C. E.; Campbell, B. T.; Chan, K. W.; Ciceri, P.; Davis, M. I.; Edeen, P. T.; Faraoni, R.; Floyd, M.; Hunt, J. P.; Lockhart, D. J.; Milanov, Z. V.; Morrison, M. J.; Pallares, G.; Patel, H. K.; Pritchard, S.; Wodicka, L. M.; Zarrinkar, P. P. A quantitative analysis of kinase inhibitor selectivity. *Nature Biotechnol.* **2008**, *26*, 127−132.

(19) Bantscheff, M.; Eberhard, D.; Abraham, Y.; Bastuck, S.; Boesche, M.; Hobson, S.; Mathieson, T.; Perrin, J.; Raida, M.; Rau, C.; Reader, V.; Sweetman, G.; Bauer, A.; Bouwmeester, T.; Hopf, C.; Kruse, U.; Neubauer, G.; Ramsden, N.; Rick, J.; Kuster, B.; Drewes, G. Quantitative chemical proteomics reveals mechanisms of action of clinical ABL kinase inhibitors. *Nature Biotechnol.* **2007**, *25*, 1035−1044.

(20) Cheng, Y.-C.; Prusoff, W. H. Relationship between the inhibition constant (IC) and the concentration of inhibitor which causes 50% inhibition (Iso) of an enzymatic reaction. *Biochem. Pharmacol.* **1973**, *22*, 3099−3108.

(21) (a) Knockaert, M.; Gray, N.; Damiens, E.; Chang, Y. T.; Grellier, P.; Grant, K.; Fergusson, D.; Mottram, J.; Soete, M.; Dubremetz, J. F.; LeRoch, K.; Doerig, C.; Schultz, P. G.; Meijer, L. Intracellular targets of cyclin-dependent kinase inhibitors: identification by affinity chromatography using immobilised inhibitors. *Chem. Biol.* **2000**, *7*, 411−422. (b) Knockaert, M.; Viking, K.; Schmitt, S.; Leost, M.; Mottram, J.; Kunick, C.; Meijer, L. Intracellular targets of paullones: identification by affinity chromatography using immobilized inhibitor. *J. Biol. Chem.* **2002**, *277*, 25493−25501. (c) Bach, S.; Knockaert, M.; Reinhardt, J.; Lozach, O.; Schmitt, S.; Baratte, B.; Koken, M.; Coburn, S. P.; Tang, L.; Jiang, T.; Liang, D. C.; Galons, H.; Dierick, J. F.; Pinna, L. A.; Meggio, F.; Totzke, F.; Schächtele, C.; Lerman, A. S.; Carnero, A.; Wan, Y.; Gray, N.; Meijer, L. Roscovitine targets, protein kinases and pyridoxal kinase. *J. Biol. Chem.* **2005**, *280*, 31208−31219.

(22) Ogawa, Y.; Nonaka, Y.; Goto, T.; Ohnishi, E.; Hiramatsu, T.; Kii, I.; Yoshida, M.; Ikura, T.; Onogi, H.; Shibuya, H.; Hosoya, T.; Ito, N.; Hagiwara, M. Development of a novel selective inhibitor of the Down syndrome-related kinase Dyrk1A. *Nature Commun.* **2010**, *1*, 1−9.

(23) Meijer, L.; Skaltsounis, A.-L.; Magiatis, P.; Polychronopoulos, P.; Knockaert, M.; Leost, M.; Ryan, X. P.; Vonica, C. A.; Brivanlou, A.; Dajani, R.; Tarricone, C.; Musacchio, A.; Roe, S. M.; Pearl, L.; Greengard, P. GSK-3 selective inhibitors derived from Tyrian purple indirubins. *Chem. Biol.* **2003**, *10*, 1255−1266. (b) Polychronopoulos, P.; Magiatis, P.; Skaltsounis, L.; Myrianthopoulos, V.; Mikros, E.; Tarricone, A.; Musacchio, A.; Roe, S. M.; Pearl, L.; Leost, M.; Greengard, P.; Meijer, L. Structural basis for the synthesis of indirubins as potent and selective inhibitors of glycogen synthase kinase-3 and cyclin-dependent kinases. *J. Med. Chem.* **2004**, *47*, 935−946.

(24) Fedorov, O.; Huber, K.; Eisenreich, A.; Filippakopoulos, P.; Bullock, A. N.; Szklarczyk, D.; Jensen, L. J.; Fabbro, D.; Trappe, J.; Rauch, U.; Bracher, F.; Knapp, S. Specific CLK inhibitors from a novel chemotype for regulation of alternative splicing. *Chem. Biol.* **2011**, *18*, 67−76.

(25) Primot, A.; Baratte, B.; Gompel, M.; Borgne, A.; Liabeuf, S.; Romette, J. L.; Costantini, F.; Meijer, L. Purification of GSK-3 by affinity chromatography on immobilised axin. *Protein Expression Purif.* **2000**, *20*, 394−404.

(26) Crawford, L. J.; Walker, B.; Ovaa, H.; Chauhan, D.; Anderson, K. C.; Morris, T. C.; Irvine, A. E. Comparative selectivity and specificity of the proteasome inhibitors BzLLLCOCHO, PS-341 and MG-132. *Cancer Res.* **2006**, *66*, 6379−6386.

(27) Leost, M.; Schultz, C.; Link, A.; Wu, Y.-Z.; Biernat, J.; Mandelkow, E.-M.; Bibb, J. A.; Snyder, G. L.; Greengard, P.; Zaharevitz, D. W.; Gussio, R.; Senderovitz, A.; Sausville, E. A.; Kunick, C.; Meijer, L. Paullones are potent inhibitors of glycogen synthase kinase-3$\beta$ and cyclin-dependent kinase 5/p25. *Eur. J. Biochem.* **2000**, *267*, 5983−5994.

(28) Yomoda, J.; Muraki, M.; Kataoka, N.; Hosoya, T.; Suzuki, M.; Hagiwara, M.; Kimura, H. Combination of Clk family kinase and SRp75 modulates alternative splicing of Adenovirus E1A. *Genes Cells* **2008**, *13*, 233−244.

(29) Jefferies, H. B.; Cooke, F. T.; Jat, P.; Boucheron, C.; Koizumi, T.; Hayakawa, M.; Kaizawa, H.; Ohishi, T.; Workman, P.; Waterfield, M. D.; Parker, P. J. A selective PIKfyve inhibitor blocks PtdIns(3,5)-P(2) production and disrupts endomembrane transport and retroviral budding. *EMBO Rep.* **2008**, *9*, 164−170.

(30) Pierre, F.; Chua, P. C.; O'Brien, S. E.; Siddiqui-Jain, A.; Bourbon, P.; Haddach, M.; Michaux, J.; Nagasawa, J.; Schwaebe, M. K.; Stefan, E.; Vialettes, A.; Whitten, J. P.; Chen, T. K.; Darjania, L.; Stansfield, R.; Anderes, K.; Bliesath, J.; Drygin, D.; Ho, C.; Omori, M.; Proffitt, C.; Streiner, N.; Trent, K.; Rice, W. G.; Ryckman, D. M. Discovery and SAR of 5-(3-chlorophenylamino)benzo[*c*][2,6]-naphthyridine-8-carboxylic acid (CX-4945), the first clinical stage

inhibitor of protein kinase CK2 for the treatment of cancer. *J. Med. Chem.* **2011**, *54*, 635−654.
(31) (a) Khoshnan, A.; Ko, J.; Watkin, E. E.; Paige, L. A.; Reinhart, P. H.; Patterson, P. H. Activation of the IkappaB kinase complex and nuclear factor-kappaB contributes to mutant huntingtin neurotoxicity. *J. Neurosci.* **2004**, *24*, 7999−8008. (b) Southwell, A. L.; Khoshnan, A.; Dunn, D. E.; Bugg, C. W.; Lo, D. C.; Patterson, P. H. Intrabodies binding the proline-rich domains of mutant huntingtin increase its turnover and reduce neurotoxicity. *J. Neurosci.* **2008**, *28*, 9013−9020. (c) Varma, H.; Voisine, C.; DeMarco, C. T.; Cattaneo, E.; Lo, D. C.; Hart, A. C.; Stockwell, B. R. Selective inhibitors of death in mutant huntingtin cells. *Nature Chem. Biol.* **2007**, *3*, 99−100. (d) Braithwaite, S. P.; Schmid, R. S.; He, D. N.; Sung, M. L.; Cho, S.; Reisnick, L.; Monaghan, M.; Hirst, W. D.; Essrich, C.; Reinhart, P. H.; Lo, D. C. Inhibition of c-Jun kinase provides neuroprotection in a model of Alzheimer's disease. *Neurobiol. Dis.* **2009**, *39*, 311−317.
(32) (a) Michell, R. H.; Dove, S. K. A protein complex that regulates PtdIns(3,5)P2 levels. *EMBO J.* **2009**, *28*, 86−87. (b) Dove, S. K.; Dong, K.; Kobayashi, T.; Williams, F. K.; Michell, R. H. Phosphatidylinositol 3,5-bisphosphate and Fab1p/PIKfyve underPPIn endo-lysosome function. *Biochem. J.* **2009**, *419*, 1−13. (c) Shisheva, A. PIKfyve: Partners, significance, debates and paradoxes. *Cell Biol. Int.* **2008**, *32*, 591−604. (d) Sbrissa, D.; Ikonomov, O. C.; Fenner, H.; Shisheva, A. ArPIKfyve homomeric and heteromeric interactions scaffold PIKfyve and Sac3 in a complex to promote PIKfyve activity and functionality. *J. Mol. Biol.* **2008**, *384*, 766−779. (e) Jin, N.; Chow, C. Y.; Liu, L.; Zolov, S. N.; Bronson, R.; Davisson, M.; Petersen, J. L.; Zhang, Y.; Park, S.; Duex, J. E.; Goldowitz, D.; Meisler, M. H.; Weisman, L. S. VAC14 nucleates a protein complex essential for the acute interconversion of PI3P and PI(3,5)P(2) in yeast and mouse. *EMBO J.* **2008**, *27*, 3221−3234. (f) Ikonomov, O. C.; Sbrissa, D.; Fenner, H.; Shisheva, A. PIKfyve−ArPIKfyve−Sac3 core complex: contact sites and their consequence for Sac3 phosphatase activity and endocytic membrane homeostasis. *J. Biol. Chem.* **2009**, *284*, 35794−35806.
(33) (a) Woods, Y. L.; Cohen, P.; Becker, W.; Jakes, R.; Goedert, M.; Wang, X.; Proud, C. G. The kinase DYRK phosphorylates protein-synthesis initiation factor eIF2Bepsilon at Ser539 and the microtubule-associated protein tau at Thr212: potential role for DYRK as a glycogen synthase kinase 3-priming kinase. *Biochem. J.* **2001**, *355*, 609−615. (b) Park, J.; Yang, E. J.; Yoon, J. H.; Chung, K. C. Dyrk1A overexpression in immortalized hippocampal cells produces the neuropathological features of Down syndrome. *Mol. Cell. Neurosci.* **2007**, *36*, 270−279. (c) Ryoo, S. R.; Jeong, H. K.; Radnaabazar, C.; Yoo, J. J.; Cho, H. J.; Lee, H. W.; Kim, I. S.; Cheon, Y. H.; Ahn, Y. S.; Chung, S. H.; Song, W. J. DYRK1A-mediated hyperphosphorylation of Tau. A functional link between Down syndrome and Alzheimer disease. *J. Biol. Chem.* **2007**, *282*, 34850−34857. (d) Wegiel, J.; Dowjat, K.; Kaczmarski, W.; Kuchna, I.; Nowicki, K.; Frackowiak, J.; Mazur Kolecka, B.; Wegiel, J.; Silverman, W. P.; Reisberg, B.; Deleon, M.; Wisniewski, T.; Gong, C. X.; Liu, F.; Adayev, T.; Chen-Hwang, M. C.; Hwang, Y. W. The role of overexpressed DYRK1A protein in the early onset of neurofibrillary degeneration in Down syndrome. *Acta Neuropathol.* **2008**, *116*, 391−407. (e) Azorsa, D. O.; Robeson, R. H.; Frost, D.; Meechoovet, B.; Brautigam, G. R.; Dickey, C.; Beaudry, C.; Basu, G. D.; Holz, D. R.; Hernandez, J. A.; Bisanz, K. M.; Gwinn, L.; Grover, A.; Rogers, J.; Reiman, E. M.; Hutton, M.; Stephan, D. A.; Mousses, S.; Dunckley, T. High-content siRNA screening of the kinome identifies kinases involved in Alzheimer's disease-related tau hyperphosphorylation. *BMC Genomics* **2010**, *11*, 25. (f) Frost, D.; Meechoovet, B.; Wang, T.; Gately, S.; Giorgetti, M.; Shcherbakova, I.; Dunckley, T. $\beta$-Carboline compounds, including harmine, inhibit DYRK1A and tau phosphorylation at multiple Alzheimer's disease-related sites. *PLoS One* **2011**, *6*, e19264. (g) Sheppard, O.; Plattner, F.; Rubin, A.; Slender, A.; Linehan, J. M.; Brandner, S.; Tybulewicz, V. L.; Fisher, E. M.; Wiseman, F. K. Altered regulation of tau phosphorylation in a mouse model of down syndrome aging. *Neurobiol. Aging* **2012**, *33* (828), e31−e44.
(34) Ryoo, S. R.; Cho, H. J.; Lee, H. W.; Jeong, H. K.; Radnaabazar, C.; Kim, Y. S.; Kim, M. J.; Son, M. Y.; Seo, H.; Chung, S. H.; Song, W. J. Dual-specificity tyrosine(Y)-phosphorylation regulated kinase 1A-mediated phosphorylation of amyloid precursor protein: evidence for a functional link between Down syndrome and Alzheimer's disease. *J. Neurochem.* **2008**, *104*, 1333−1344.
(35) Ryu, Y. S.; Park, S. Y.; Jung, M. S.; Yoon, S. H.; Kwen, M. Y.; Lee, S. Y.; Choi, S. H.; Radnaabazar, C.; Kim, M. K.; Kim, H; Kim, K.; Song, W. J.; Chung, S. H. Dyrk1A-mediated phosphorylation of Presenilin 1: a functional link between Down syndrome and Alzheimer's disease. *J. Neurochem.* **2010**, *115*, 574−584.
(36) Sitz, J. H.; Baumgärtel, K.; Hämmerle, B.; Papadopoulos, C.; Hekerman, P.; Tejedor, F. J.; Becker, W.; Lutz, B. The Down syndrome candidate dual-specificity tyrosine phosphorylation-regulated kinase 1A phosphorylates the neurodegeneration-related septin 4. *Neuroscience* **2008**, *157*, 596−605.
(37) Jung, M. S.; Park, J. H.; Ryu, Y. S.; Choi, S. H.; Yoon, S. H.; Kwen, M. Y.; Oh, J. Y.; Song, W. J.; Chung, S. H. Regulation of RCAN1 protein activity by Dyrk1A protein-mediated phosphorylation. *J. Biol. Chem.* **2011**, *286*, 40401−40412.
(38) Park, J. H.; Jung, M. S.; Kim, Y. S.; Song, W. J.; Chung, S. H. Phosphorylation of Munc18-1 byDyrk1A regulates its interaction with Syntaxin 1 and X11$\alpha$. *J. Neurochem.* **2012**, *122*, 1081−1091.
(39) (a) Ferrer, I.; Barrachina, M.; Puig, B.; Martinez de Lagran, M.; Marti, E.; Avila, J.; Dierssen, M. Constitutive Dyrk1A is abnormally expressed in Alzheimer disease, Down syndrome, Pick disease, and related transgenic models. *Neurobiol. Dis.* **2005**, *20*, 392−400. (b) Kimura, R.; Kamino, K.; Yamamoto, M.; Nuripa, A.; Kida, T.; Kazui, H.; Hashimoto, R.; Tanaka, T.; Kudo, T.; Yamagata, H.; Tabara, Y.; Miki, T.; Akatsu, H.; Kosaka, K.; Funakoshi, E.; Nishitomi, K.; Sakaguchi, G.; Kato, A.; Hattori, H.; Uema, T.; Takeda, M. The DYRK1A gene, encoded in chromosome 21 Down syndrome critical region, bridges between {beta}-amyloid production and tau phosphorylation in Alzheimer disease. *Hum. Mol. Genet.* **2007**, *16*, 15−23.
(40) (a) Altafaj, X.; Dierssen, M.; Baamonde, C.; Marti, E.; Visa, J.; Guimera, J.; Oset, M.; Gonzalez, J. R.; Florez, J.; Fillat, C.; Estivill, X. Neurodevelopmental delay, motor abnormalities and cognitive deficits in transgenic mice overexpressing Dyrk1A (minibrain), a murine model of Down's syndrome. *Hum. Mol. Genet.* **2001**, *10*, 1915−1923. (b) Arron, J. R.; Winslow, M. M.; Polleri, A.; Chang, C. P.; Wu, H.; Gao, X.; Neilson, J. R.; Chen, L.; Heit, J. J.; Kim, S. K.; Yamasaki, N.; Miyakawa, T.; Francke, U.; Graef, I. A.; Crabtree, G. R. NFAT dysregulation by increased dosage of DSCR1 and DYRK1A on chromosome 21. *Nature* **2006**, *441*, 595−600. (c) Guedj, F.; Sébrié, C.; Rivals, I.; Ledru, A.; Paly, E.; Bizot, J. C.; Smith, D.; Rubin, E.; Gillet, B.; Arbones, M.; Delabar, J. M. Green tea polyphenols rescue of brain defects induced by overexpression of DYRK1A. *PLoS One* **2009**, *4*, e4606.
(41) (a) Shi, J.; Zhang, T.; Zhou, C.; Chohan, M. O.; Gu, X.; Wegiel, J.; Zhou, J.; Hwang, Y. W.; Iqbal, K.; Grundke-Iqbal, I.; Gong, C. X.; Liu, F. Increased dosage of Dyrk1A alters alternative splicing factor (ASF)-regulated alternative splicing of tau in Down syndrome. *J. Biol. Chem.* **2008**, *283*, 28660−28669. (b) Qian, W.; Liang, H.; Shi, J.; Jin, N.; Grundke-Iqbal, I.; Iqbal, K.; Gong, C. X.; Liu, F. Regulation of the alternative splicing of tau exon 10 by SC35 and Dyrk1A. *Nucleic Acids Res.* **2011**, *39*, 6161−6171. (c) Wegiel, J.; Kaczmarski, W.; Barua, M.; Kuchna, I.; Nowicki, K.; Wang, K. C.; Wegiel, J.; Yang, S. M.; Frackowiak, J.; Mazur-Kolecka, B.; Silverman, W. P.; Reisberg, B.; Monteiro, I.; de Leon, M.; Wisniewski, T.; Dalton, A.; Lai, F.; Hwang, Y. W.; Adayev, T.; Liu, F.; Iqbal, K.; Iqbal, I. G.; Gong, C. X. Link between DYRK1A overexpression and several-fold enhancement of neurofibrillary degeneration with 3-repeat tau protein in Down syndrome. *J. Neuropathol. Exp. Neurol.* **2011**, *70*, 36−50. (d) Yin, X.; Jin, N.; Gu, J.; Shi, J.; Gong, C. X.; Iqbal, K.; Grundke-Iqbal, I.; Liu, F. Dual-specificity-tyrosine-phosphorylated and regulated kinase 1A (Dyrk1A) modulates serine−arginine rich protein 55 (SRp55)-promoted tau exon 10 inclusion. *J. Biol. Chem.* **2012**, *287*, 30497−30506. (e) Ding, S.; Shi, J.; Qian, W.; Iqbal, K.; Grundke-Iqbal, I.;

Gong, C. X.; Liu, F. Regulation of alternative splicing of tau exon 10 by 9G8 and Dyrk1A. *Neurobiol. Aging* **2012**, *33*, 1389−1399.
(42) Glatz, D. C.; Rujescu, D.; Tang, Y.; Berendt, F. J.; Hartmann, A. M.; Faltraco, F.; Rosenberg, C.; Hulette, C.; Jellinger, K.; Hampel, H.; Riederer, P.; Möller, H. J.; Andreadis, A.; Henkel, K.; Stamm, S. The alternative splicing of tau exon 10 and its regulatory proteins CLK2 and TRA2-BETA1 changes in sporadic Alzheimer's disease. *J. Neurochem.* **2006**, *96*, 635−644.
(43) (a) Twine, N. A.; Janitz, K.; Wilkins, M. R.; Janitz, M. Whole transcriptome sequencing reveals gene expression and splicing differences in brain regions affected by Alzheimer's disease. *PLoS One* **2011**, *6*, e16266. (b) Tollervey, J. R.; Wang, Z.; Hortobágyi, T.; Witten, J. T.; Zarnack, K.; Kayikci, M.; Clark, T. A.; Schweitzer, A. C.; Rot, G.; Curk, T.; Zupan, B.; Rogelj, B.; Shaw, C. E.; Ule, J. Analysis of alternative splicing associated with aging and neurodegeneration in the human brain. *Genome Res.* **2011**, *21*, 1572−1582. (c) Massone, S.; Vassallo, I.; Castelnuovo, M.; Fiorino, G.; Gatta, E.; Robello, M.; Borghi, R.; Tabaton, M.; Russo, C.; Dieci, G.; Cancedda, R.; Pagano, A. RNA polymerase III drives alternative splicing of the potassium channel-interacting protein contributing to brain complexity and neurodegeneration. *J. Cell Biol.* **2011**, *193*, 851−866. (d) Scott, H. A.; Gebhardt, F. M.; Mitrovic, A. D.; Vandenberg, R. J.; Dodd, P. R. Glutamate transporter variants reduce glutamate uptake in Alzheimer's disease. *Neurobiol. Aging* **2011**, *32* (553), e1−e11. (e) Ishunina, T. A.; Swaab, D. F. Decreased alternative splicing of estrogen receptor-$\alpha$ mRNA in the Alzheimer's disease brain. *Neurobiol Aging* **2012**, *33*, 286−296. (f) Fisette, J. F.; Montagna, D. R.; Mihailescu, M. R.; Wolfe, M. S. A G-rich element forms a G-quadruplex and regulates BACE1 mRNA alternative splicing. *J. Neurochem.* **2012**, *121*, 763−773.
(44) (a) Medina, M.; Avila, J. Glycogen synthase kinase-3 (GSK-3) inhibitors for the treatment of Alzheimer's disease. *Curr. Pharm. Des.* **2010**, *1*, 2790−2798. (b) Hernández, F.; Gómez de Barreda, E.; Fuster-Matanzo, A.; Lucas, J. J.; Avila, J. GSK3: a possible link between beta amyloid peptide and tau protein. *Exp. Neurol.* **2010**, *223*, 322−325. (c) Eldar-Finkelman, H. Martinez, A. GSK-3 Inhibitors: Preclinical and Clinical Focus on CNS. *Front. Mol. Neurosci.* **2011**, *4*, 32. (d) Kremer, A.; Louis, J. V.; Jaworski, T.; Van Leuven, F. GSK3 and Alzheimer's Disease: Facts and Fiction... *Front. Mol. Neurosci.* **2011**, *4*, 17.
(45) (a) Domínguez, J. M.; Fuertes, A.; Orozco, L.; del Monte-Millán, M.; Delgado, E.; Medina, M. Evidence for irreversible inhibition of glycogen synthase kinase-3$\beta$ by tideglusib. *J. Biol. Chem.* **2012**, *287*, 893−904. (b) Martinez, A.; Gil, C.; Perez, D. I. Glycogen synthase kinase 3 inhibitors in the next horizon for Alzheimer's disease treatment. *Int. J. Alzheimer's Dis.* **2011**, *2011*, 280502. (c) Palomo, V.; Perez, D. I.; Perez, C.; Morales-Garcia, J. A.; Soteras, I.; Alonso-Gil, S.; Encinas, A.; Castro, A.; Campillo, N. E.; Perez-Castillo, A.; Gil, C.; Martinez, A. 5-Imino-1,2,4-thiadiazoles: first small molecules as substrate competitive inhibitors of glycogen synthase kinase 3. *J. Med. Chem.* **2012**, *55*, 1645−1661.
(46) (a) De Felice, F. G.; Vieira, M. N.; Bomfim, T. R.; Decker, H.; Velasco, P. T.; Lambert, M. P.; Viola, K. L.; Zhao, W. Q.; Ferreira, S. T.; Klein, W. L. Protection of synapses against Alzheimer's-linked toxins: insulin signaling prevents the pathogenic binding of Abeta oligomers. *Proc. Natl. Acad. Sci. U.S.A.* **2009**, *106*, 1971−1976. Erratum in: *Proc. Natl. Acad. Sci. U.S.A.* **2009**, *106*, 7678. (b) Pigino, G.; Morfini, G.; Atagi, Y.; Deshpande, A.; Yu, C.; Jungbauer, L.; LaDu, M.; Busciglio, J.; Brady, S. Disruption of fast axonal transport is a pathogenic mechanism for intraneuronal amyloid beta. *Proc. Natl. Acad. Sci. U.S.A.* **2009**, *106*, 5907−5912. (c) Perez, D. I.; Gil, C.; Martinez, A. Protein kinases CK1 and CK2 as new targets for neurodegenerative diseases. *Med. Res. Rev.* **2011**, *31*, 924−954.
(47) (a) Tsuruta, F.; Green, E. M.; Rousset, M.; Dolmetsch, R. E. PIKfyve regulates CaV1.2 degradation and prevents excitotoxic cell death. *J. Cell Biol.* **2009**, *187*, 279−294. (b) Zhang, Y.; Zolov, S. N.; Chow, C. Y.; Slutsky, S. G.; Richardson, S. C.; Piper, R. C.; Yang, B.; Nau, J. J.; Westrick, R. J.; Morrison, S. J.; Meisler, M. H.; Weisman, L. S. Loss of Vac14, a regulator of the signaling lipid phosphatidylinositol 3,5-bisphosphate, results in neurodegeneration in mice. *Proc. Natl. Acad. Sci. U.S.A.* **2007**, *104*, 17518−17523. (c) Li, S.; Tiab, L.; Jiao, X.; Munier, F. L.; Zografos, L.; Frueh, B. E.; Sergeev, Y.; Smith, J.; Rubin, B.; Meallet, M. A.; Forster, R. K.; Hejtmancik, J. F.; Schorderet, D. F. Mutations in PIP5K3 are associated with François−Neetens mouchetée fleck corneal dystrophy. *Am. J. Hum. Genet.* **2005**, *77*, 54−63.
(48) (a) Chow, C. Y.; Zhang, Y.; Dowling, J. J.; Jin, N.; Adamska, M.; Shiga, K.; Szigeti, K.; Shy, M. E.; Li, J.; Zhang, X.; Lupski, J. R.; Weisman, L. S.; Meisler, M. H. Mutation of FIG4 causes neurodegeneration in the pale tremor mouse and patients with CMT4J. *Nature* **2007**, *448*, 68−72. (b) Lenk, G. M.; Ferguson, C. J.; Chow, C. Y.; Jin, N.; Jones, J. M.; Grant, A. E.; Zolov, S. N.; Winters, J. J.; Giger, R. J.; Dowling, J. J.; Weisman, L. S.; Meisler, M. H. Pathogenic mechanism of the FIG4 mutation responsible for Charcot−Marie−Tooth disease CMT4J. *PLoS Genet.* **2011**, e1002104. (c) Ferguson, C. J.; Lenk, G. M.; Jones, J. M.; Grant, A. E.; Winters, J. J.; Dowling, J. J.; Giger, R. J.; Meisler, M. H. Neuronal expression of Fig4 is both necessary and sufficient to prevent spongiform neurodegeneration. *Hum. Mol. Genet.* **2012**, *21*, 3525−3534. (d) Nicholson, G.; Lenk, G. M.; Reddel, S. W.; Grant, A. E.; Towne, C. F.; Ferguson, C. J.; Simpson, E.; Scheuerle, A.; Yasick, M.; Hoffman, S.; Blouin, R.; Brandt, C.; Coppola, G.; Biesecker, L. G.; Batish, S. D.; Meisler, M. H. Distinctive genetic and clinical features of CMT4J: a severe neuropathy caused by mutations in the PI(3,5)$P_2$ phosphatase FIG4. *Brain* **2011**, *134*, 1959−1971.
(49) Bullock, A. N.; Debreczeni, J.; Amos, A. L.; Knapp, S.; Turk, B. E. Structure and substrate specificity of the Pim-1 kinase. *J. Biol. Chem.* **2005**, *280*, 41675−41682.
(50) Dajani, R.; Fraser, E.; Roe, S. M.; Yeo, M.; Good, V. M.; Thompson, V.; Dale, T. C.; Pearl, L. H. Structural basis for recruitment of glycogen synthase kinase 3$\beta$ to the axin-APC scaffold complex. *EMBO J.* **2003**, *22*, 494−501.
(51) Leslie, A. G. W.; Powell, H. R. Evolving methods for macromolecular crystallography; Springer: Berlin, 2007; Vol. *245*, pp 41−51.
(52) Evans, P. Scaling and assessment of data quality. *Acta Crystallogr., Sect. D: Biol. Crystallogr.* **2006**, *D62*, 72−82.
(53) McCoy, A. J.; Grosse-Kunstleve, R. W.; Adams, P. D.; Winn, M. D.; Storoni, L. C.; Read, R. J. Phaser crystallographic software. *J. Appl. Crystallogr.* **2007**, *40*, 658−674.
(54) Emsley, P.; Lohkamp, B.; Scott, W. G.; Cowtan, K. Features and development of Coot. *Acta Crystallogr., Sect. D: Biol. Crystallogr.* **2010**, *66*, 486−501.
(55) Murshudov, G. N.; Vagin, A. A.; Dodson, E. J. Refinement of macromolecular structures by the maximum-likelihood method. *Acta Crystallogr., Sect. D: Biol. Crystallogr.* **1997**, *D53*, 240−255.
(56) Kabsch, W. XDS. *Acta Crystallogr., Sect. D: Biol. Crystallogr.* **2010**, *66*, 125−132.
(57) Adams, P. D.; Afonine, P. V.; Bunkóczi, G.; Chen, V. B.; Davis, I. W.; Echols, N.; Headd, J. J.; Hung, L. W.; Kapral, G. J.; Grosse-Kunstleve, R. W.; McCoy, A. J.; Moriarty, N. W.; Oeffner, R.; Read, R. J.; Richardson, D. C.; Richardson, J. S.; Terwilliger, T. C.; Zwart, P. H. PHENIX: a comprehensive Python-based system for macromolecular structure solution. *Acta Crystallogr., Sect. D: Biol. Crystallogr.* **2010**, *66*, 213−221.
(58) Berman, H. M.; Westbrook, J.; Feng, Z.; Gilliland, G.; Bhat, T. N.; Weissig, H.; Shindyalov, I. N.; Bourne, P. E. The Protein Data Bank. *Nucleic Acids Res.* **2000**, *28*, 235−242.
(59) Conradt, L.; Godl, K.; Schaab, C.; Tebbe, A.; Eser, S.; Diersch, S.; Michalski, C. W.; Kleeff, J.; Schnieke, A.; Schmid, R. M.; Saur, D.; Schneider, G. Disclosure of Erlotinib as a multikinase inhibitor in pancreatic ductal adenocarcinoma. *Neoplasia* **2011**, *13*, 1026−1034.
(60) Boersema, P. J.; Raijmakers, R.; Lemeer, S.; Mohammed, S.; Heck, A. J. Multiplex peptide stable isotope dimethyl labeling for quantitative proteomics. *Nature Protoc.* **2009**, *4*, 484−494.
(61) Rappsilber, J.; Mann, M.; Ishihama, Y. Protocol for micro-purification, enrichment, pre-fractionation and storage of peptides for proteomics using StageTips. *Nature Protoc.* **2007**, *2*, 1896−1906.

(62) Olsen, J. V.; de Godoy, L. M.; Li, G.; Macek, B.; Mortensen, P.; Pesch, R.; Makarov, A.; Lange, O.; Horning, S.; Mann, M. Parts per million mass accuracy on an Orbitrap mass spectrometer via lock mass injection into a C-trap. *Mol. Cell Proteomics* **2005**, *4*, 2010−2021.
(63) Cox, J.; Mann, M. MaxQuant enables high peptide identification rates, individualized ppb-range mass accuracies and proteome-wide protein quantification. *Nature Biotechnol.* **2008**, *26*, 1367−1372.
(64) Cox, J.; Neuhauser, N.; Michalski, A.; Scheltema, R. A.; Olsen, J. V.; Mann, M. Andromeda: a peptide search engine integrated into the MaxQuant environment. *J. Proteome Res.* **2011**, *10*, 1794−1805.
(65) Ribas, J.; Boix, J. Cell differentiation, caspase inhibition, and macromolecular synthesis blockage, but not BCL-2 or BCL-XL proteins, protect SH-SY5Y cells from apoptosis triggered by two CDK inhibitory drugs. *Exp. Cell Res.* **2004**, *295*, 9−24.
(66) Murata, S.; Yoshiara, T.; Lim, C. R.; Sugino, M.; Kogure, M.; Ohnuki, T.; Komurasaki, T.; Matsubara, K.. Psychophysiological stress regulated gene expression in mice. *FEBS Lett.* **2005**, *579*, 2137−2142.
(67) (a) Yacoubian, T. A.; Lo, D. C. Truncated and full-length TrkB receptors regulate distinct modes of dendritic growth. *Nature Neurosci.* **2000**, *3*, 342−349. (b) Wang, J. K.; Portbury, S.; Thomas, M. B.; Barney, S.; Ricca, D. J.; Morris, D. L.; Warner, D. S.; Lo, D. C. Cardiac glycosides provide neuroprotection against ischemic stroke: discovery by a brain slice-based compound screening platform. *Proc. Natl. Acad. Sci. U.S.A.* **2006**, *103*, 10461−10466. (c) Lo, D. C. Neuronal transfection using particle-mediated gene transfer. *Curr. Protoc. Neurosci.* **1999**, *3*, 1−12.